2009-01-01

# Finite Element Modeling Of Nondestructive Test Methods Used For Detection Of Delamination In Hot Mix Asphalt Pavements

Dante Mejia Munoz
*University of Texas at El Paso*, dmejia4@miners.utep.edu

# FINITE ELEMENT MODELING OF NONDESTRUCTIVE TEST METHODS USED FOR DETECTION OF DELAMINATION IN HOT MIX ASPHALT PAVEMENTS

DANTE MEJIA MUNOZ

Department of Civil Engineering

APPROVED:

Soheil Nazarian, Ph.D., Chair

Cesar Carrasco, Ph.D.

Louis J. Everett, Ph.D.

Carlos Martin Chang-Albitres, Ph.D.

Patricia D. Witherspoon, Ph.D.
Dean of the Graduate School

# Dedication

I would like to dedicate my Thesis to my mother who always encouraged me to look forward no matter what and because she always believed in me to acquire all my goals. To my father who lead me to the amazing world of civil engineering and because his insistence to go beyond of the bachelor degree. To my brothers and sister whom always gave me support and shared their knowledge. To my wife who supported me emotionally, she gave me all hope I needed in adverse times and especially for all her unconditional love.

# FINITE ELEMENT MODELING OF NONDESTRUCTIVE TEST METHODS USED FOR DETECTION OF DELAMINATION IN HOT MIX ASPHALT PAVEMENTS

by

DANTE MEJIA MUNOZ, B.S.C.E.

THESIS

Presented to the Faculty of the Graduate School of

The University of Texas at El Paso

in Partial Fulfillment

of the Requirements

for the Degree of

MASTER OF SCIENCE

Department of Civil Engineering

THE UNIVERSITY OF TEXAS AT EL PASO

August 2009

## Acknowledgements

I would like to show my most sincere gratitude to Dr. Nazarian, who served as an excellent advisor and mentor. He showed in me the potential to do research and lead me to the world of science. He was always available to provide guidance for the solution of problems and without him this Thesis would not be possible. To Mr. Manuel Celaya for his wonderful friendship, for his guidance trough my entire Thesis and for encouraging me in his own peculiar way. To Mr. Imad Abdallah who received me at CTIS with open arms and for providing me all I needed for my Thesis. To Dr. Deren Yuan for sharing his extensive knowledge. To the entire CTIS staff whom I considered as a family. Special thanks to Mr. Jose Luis Hernandez, Mr. Hector Hernandez, Mr. Enrique Portillo and to Mr. Braulio Garcia whom provided me all the information I requested from my results when I was far away from my computer. And to Mr. Carlos Solis who virtually was an extension of my body and helped me on the most critical part on my project, the ending.

# Abstract

The importance of the detection of delamination of Hot Mix Asphalt Pavements at an early stage, will result in a longer service life of the structure. Recently Nondestructive methods have been employed for the detection of delamination.

This study will focus on three of these methods: Impact Echo, Ultrasonic Surface Waves and Impulse response. By using a Finite Element software, the behavior of these three methods was evaluated and then a parametric study was elaborated. The parametric study shows the impact of different variables related to the properties of the flexible pavement and the delamination.

# Table of Contents

# List of Tables

# List of Figures

# Chapter 1: Introduction

Delamination of Hot Mix Asphalt (HMA) in flexible pavements is a serious problem that can negatively affect the performance of pavements and decrease their remaining service lives. Delamination occurs when the bond between adjacent HMA layers is nonexistent or weak producing a sliding between layers and thus creating flaws such as slippage and potholes. Delamination is due to several causes, but it is mainly related to problems on the bonding agent (tack coat) used for that purpose. Lack of or inappropriate application of tack coat between layers, or the use of a deficient products as a bonding agent, are assumed as the typical causes that lead to delamination.

The presence of delamination in HMA pavements can currently be detected visually once the pavement surface exhibits a distress. A number of cores are then extracted to corroborate that the failure in the HMA is caused by delamination. However, the process of coring is time consuming and rather expensive. For that reason new nondestructive testing (NDT) methods for the detection of delamination are highly desirable. Three of these methods that have shown promising results in the detection of delamination are the Impact Echo (IE), Ultrasonic Surface Waves (USW) and the Impulse Response (IR) methods. On the other hand, results (signals) obtained from these methods can vary depending on the properties of the asphalt which can complicate the interpretation of these results.

To gain a better understanding of the signals obtained from the IE, USW and IR methods a numerical study utilizing finite element method (FEM) was carried out to complete this study. The FEM was employed to reproduce the time records that would be observed in the field for intact, debonded and delaminated HMA layers. The impact of the pavement layer properties such as the modulus and thickness of the HMA and supporting layers (base and subgrade) were also studied.

## 1.1 OBJECTIVES

The goal of this study was to develop a parametric study based on the detection of delamination in HMA pavements by using the IE, USW and IR methods. To carry out the parametric study, a series of FEM models were developed with different degrees of debonding and pavement properties.

## 1.2 ORGANIZATION

Following this Introduction, Chapter Two provides a review of literature related to delamination in flexible pavements, a description of the characteristics and principles of non-destructive methods, mainly IE, USW and IR, for detection of delamination and the finite element method.

Chapter Three provides a detailed description of the criteria for the parameters that were taken into account to define the finite element models used in this study, and the criteria used for the parametric study.

Chapter Four contains the results obtained from the IE, USW and IR methods using the finite element method and an evaluation of the analyses.

Chapter Five presents conclusions of the study and future recommendations.

# Chapter 2: Literature Review

Delamination is a mode of failure of layered materials when the two adjacent layers do not function as one continuous unit either due to separation or weak bond. In flexible pavements two types of delamination can occur: delamination between HMA layers and delamination between base course and HMA. Both types negatively impact the structural and functional performance of the pavement. However, the debonding at the interfaces of HMA layers is more critical. Even though delamination at any depth is undesirable, some studies have found that under truck traffic, delamination deeper than 200 mm (8 in.) less significantly impact the structure of the pavement, with less possibility for a surface distress (Hammons et al., 2005). Therefore the focus of the detection of delamination should be on layers close to the surface.

Delamination is originated by several causes such as lack of bonding agent (tack coat), an incorrect application of bonding agent, the use of a low quality bonding agent, improper construction technique, or lack of proper compaction (Mejia et al., 2009). It is further expanded by repeated cyclic stresses or an impact producing separation between layers. This usually happens in areas where the vehicles are more likely to apply horizontal forces such as at intersections, steep ramps and small radius curves (Romanoschi and Metcalf, 2002). When delamination problems are not detected in early stages, slippage failures commonly develop. Slippage is described as crescent or half-moon-shaped cracks having two ends pointed away from the direction of the traffic (Shanin et al, 1986) as shown in Figure 2.1.

Few studies have been carried out on adhesion properties of the various layers of flexible pavements or on the overall influence of the bonding conditions between layers. Some studies have concluded that asphalt layer thickness plays a key role in preventing delamination. Increasing layer thickness reduces the interfacial shear stress, due to vertical and horizontal loads (Kulkarni, 2004). Other authors have noted that weak bonding between bituminous pavement layers may develop during construction due to poor quality control, lack of tack coat, contamination of the lower layer or laying in cold weather (Kruntcheva et al., 2006).

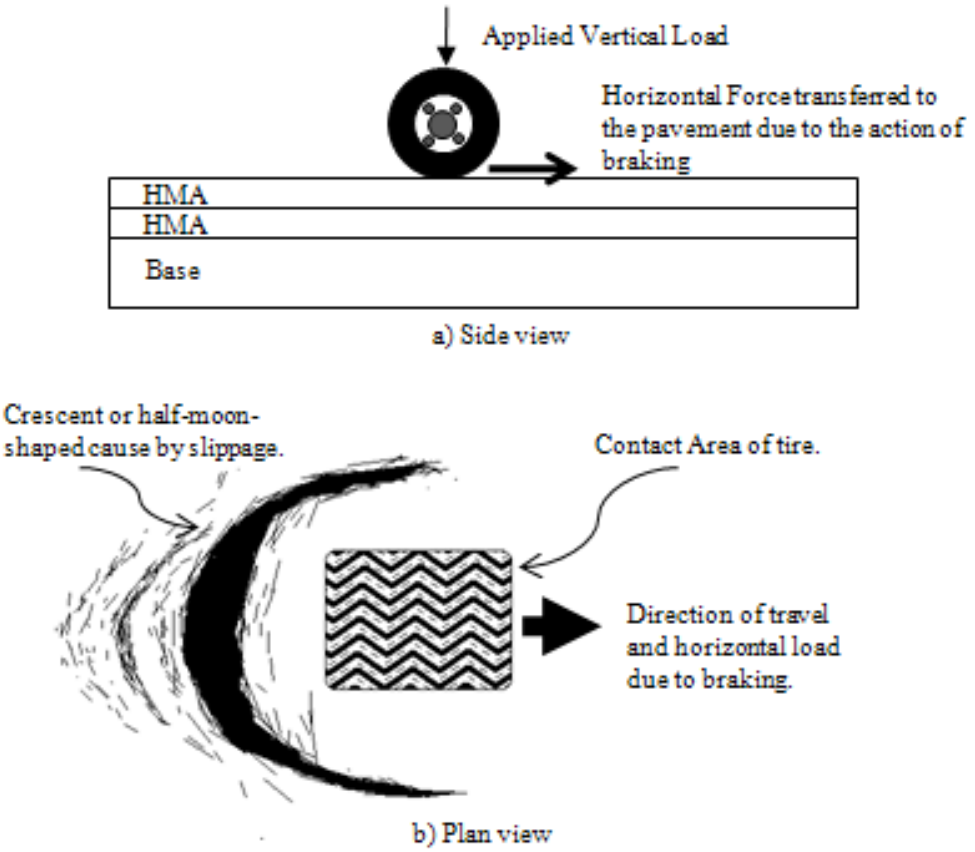


Figure 2.1: Typical Slippage Failure.

Romanoschi and Metcalf (2000) conducted a study for the characterization of asphalt concrete layer interfaces. In that study three parameters were considered to describe the interface behavior: the interface reaction modulus, the shear strength and the friction coefficient after failure. Test sections, with and without tack coat, were constructed comprising of a binder course and a wearing course of 50 mm (2 in.) and 40 mm (1.6 in.) in thickness, respectively. Direct shear tests at a constant normal load were performed on cores obtained from these sections. This research led to the following findings: (1) all three parameters are temperature dependant; (2) for the interface with tack coat, normal stress did not affect the reaction modulus and the shear modulus but for the interface without tack coat these parameters were affected.

Canestrari et al. (2005) conducted a study for the characterization of interlayer shear resistance. They pointed out to the importance of appropriate compaction comparing cores from a trial section versus laboratory samples. Since air voids from laboratory samples were lower than those from their

section cores, a higher cohesion and shear resistance were obtained from laboratory specimens. These results seem to confirm that interlayer shear resistance also depends on the air void content of the mixes.

## 2.1 NON-DESTRUCTIVE METHODS FOR DETECTION OF DELAMINATION OF HMA

A number of NDT technologies have been developed that have the potential for detection of delamination within HMA layers. Most of these technologies have been used extensively for detecting delamination in Portland cement concrete (PCC) slabs rather than HMA layers. The detection of delamination in PCC is much more straightforward than in the HMA. Some of the difficulties for the detection of delamination in HMA are: HMA layers are placed in thinner lifts, HMA is not considered as a homogenous material since it behaves more like a particulate matter, and the properties of the HMA are highly temperature-dependent.

The desirable method should ideally detect the onset of delamination as soon as possible, as opposed to detecting the problems in its advanced stages. Therefore, an appropriate practical nondestructive tool capable of detecting the potential of delamination or debonding during or shortly after construction is desirable. Three methods have shown promising results: IE, USW and IR methods. For the understanding of these methods a description of their principles is provided in the following sections.

### 2.1.1 Principles of Wave Propagation.

When the surface of an object is impacted, waves propagate through them. These waves are called stress waves and they are divided in three different types: compression waves, shear waves and surface waves. The compression and shear waves move through the solid along a spherical front. The surface waves, as the name states, propagate along the surface of the solid.

The velocity of the compression waves or P-waves in an infinite isotropic, elastic medium is given by the following equation:

$$C_c = \sqrt{\frac{E(1-\nu)}{\rho(1+\nu)(1-2\nu)}} \tag{1.1}$$

where *Cc* is the velocity of the P-wave, *E* is the modulus of elasticity, *v* is the Poisson's ratio and $\rho$ is the mass density.

In a medium where the material is restricted from deformation in two lateral directions, the ratio of axial strain is known as constrained modulus (Baker, 1995). The constrained modulus, *M*, is given by the following equation:

$$M = \rho C_C^2 \tag{1.2}$$

The shear wave or S-wave, which propagates at a lower velocity than the P-wave, is given by the following equation:

$$C_s = \sqrt{\frac{G}{\rho}} = \sqrt{\frac{E}{\rho 2(1+v)}} \tag{1.3}$$

where *G* is the shear modulus of elasticity.

The ratio between the P-wave and S-wave velocities is given by the following equation:

$$\frac{Cs}{Cc} = \sqrt{\frac{1-2v}{2(1-v)}} \tag{1.4}$$

Surface waves, which carry about two-thirds of the seismic energy generated within a layer, are of higher amplitudes and attenuate at a lower rate than body waves. R-waves propagate at a speed of approximately 90 percent of S-waves.

When a stress wave is propagating through a layered material, a portion of the wave is reflected at each layer interface. The amplitude of a reflected wave is a function of the angle of incidence. If the angle of incidence is 90º (normal incidence), the amplitude of the reflected wave is maximum. The normal incidence is related to the specific acoustic impedance of the material and a coefficient is given by the following equation:

$$R = \frac{Z_2 - Z_1}{Z_2 + Z_1} \tag{1.5}$$

where $R$ is the reflection coefficient, $Z_2$ is the specific acoustic impedance of Material 2, and $Z_1$ is the specific acoustic impedance of Material 1. The specific acoustic impedance is the product of the wave speed and the density of the material. Therefore when a stress wave is propagating through a material like concrete with very high specific acoustic impedance, and encounters air with very low specific acoustic impedance, the reflected wave has almost the same energy as the incident wave.

### 2.1.1 Impact Echo

Impact Echo is an acoustic method for nondestructive evaluation that can be used for concrete and asphalt layers. The method became popular in the mid-1980's due to work by Sansalone and Carino (1984). Impact echo is based on the propagation of stress waves generated by a mechanical impact. The impact has a short duration and is produced by tapping the surface of the pavement. A receiver-transducer records the surface displacement caused by the stress waves reflected from a flaw or an interface (Figure 2.2a). The signal is sent to a data acquisition system and then processed using a computer (Figure 2.2b). If the receiver is placed at an adequate distance from the impact, the P-waves reflected will dominate the response and the resulting displacement versus time is obtained (Figure 2.2c). This time-domain records are transformed into the frequency domain using the fast Fourier transform (FFT) to facilitate the analysis of the signal (Figure 2.2d).

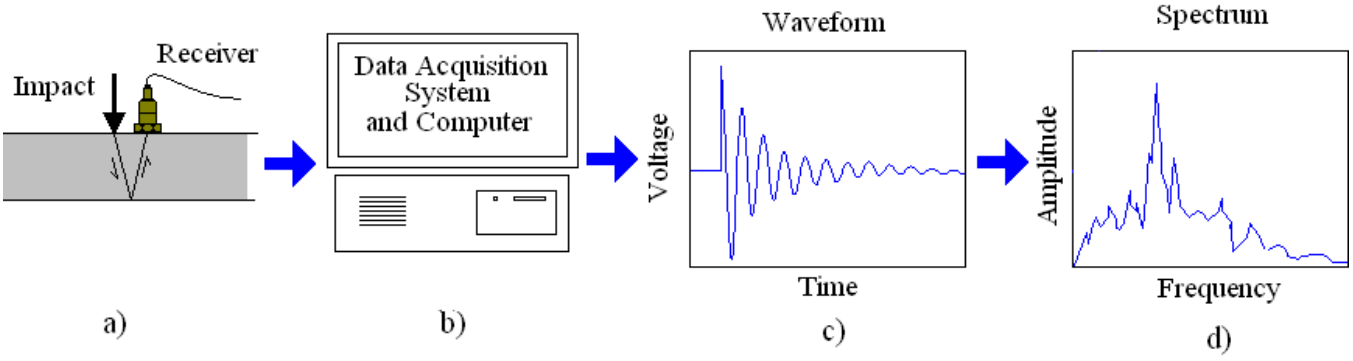


Figure 2.2: A Diagram of the Impact Echo Method.

The frequency domain analysis can be explained as follows. When the surface of a homogeneous material is impacted, the P-wave creates multiple reflections between the impacted surface and the reflecting interface. The reflected waveform has a periodic pattern that depends on the round-trip travel distance of the P-wave. The time interval between every arrival of the reflected P-wave represents the distance traveled divided by the velocity of the wave. The frequency of the P-wave can be defined as the inverse of the time interval and is given by the following equation (Carino, 2001):

$$f = \frac{C_C}{2h} \tag{1.6}$$

where $f$ is the return frequency of the P-wave and $h$ is the distance between the impacted surface and the reflecting interface.

Several studies have been carried out for detection of flaws using the IE method. A study conducted by Sansalone and Streett (1997) showed that P-waves from surface of large cracks or voids dominated the response and the waveform and spectrum obtained appeared very similar to those from a solid plate having a thickness equal to the depth of the flaw. The spectrum showed a single large amplitude peak corresponding to the depth of the flaw. In the case of cracks or voids with small lateral dimensions, the P-waves were both reflected from the surface and diffracted around the edges of the cracks. The diffracted waves travel below the crack and are eventually reflected from bottom surface traveling back up and are again diffracted for the crack before they reach the top surface. In that case, the spectrum exhibited two distinct peaks: a low-amplitude, high-frequency peak which corresponded to the depth of the crack and a high-amplitude, low-frequency peak which corresponded to the thickness of the plate.

### 2.1.2 Ultrasonic Surface Waves

The Ultrasonic Surface Wave (USW) method uses the surface wave dispersive characteristics or elastic properties as an indication of the condition of the material tested. In this method, the wave energies are confined to very high frequencies and therefore the shear wave velocity profile within the topmost layer is resulted (Nazarian et al., 1993). In the USW, the variation in the phase velocity with wavelength, called a dispersion curve, is generated (Yuan, 2000). At wavelengths less than or equal to

the thickness of the uppermost layer, the velocity of propagation of surface waves is more or less independent of wavelength. Assuming that the properties of the uppermost layer are uniform, if one simply generates high-frequency (short-wavelength) waves, the phase velocity of the upper layer can be determined.

The wavelength at which the phase velocity is no longer constant is closely related to the thickness of the top layer (Nazarian et al., 1997). For two layers with similar modulus bonded together, the variation in modulus with depth is more or less constant. However, when the two layers are debonded, the variation in modulus with depth is significantly reduced below the interface of the two layers. This principle can be readily used to not only detect but also identify the approximate depth of the debonded layers. This method has been successfully used in a few forensic studies to detect HMA debonding.

A forensic study carried out by Hammons et al. (2005) showed the applicability of the USW method to HMA pavements. As an example, typical dispersion curves (the variations in modulus versus depth) obtained through the USW analysis from locations of an intact and a damaged core are shown in Figure 2.3. The dispersion curve for the intact core would have been constant if different lifts were of the same material. However, at least four different lifts can be identified in the first 12 in. of the intact core. The top layer (first 4 inches) is significantly stiffer than the rest. From 4 to 6 in., the material seems to be of lower quality and below 6 in. the modulus increases again. In the case of the damaged core, the top 4 in. seem to be stiffer. A significant drop in modulus is observed at a wavelength of 4 in. where some loss of material was found due to stripping. The modulus increases again at a depth of 6 in.

Nazarian et al. (1993) developed an automated testing equipment known as the Seismic Pavement Analyzer (SPA). Later, the same technology was implemented in portable hand-held device called the Portable Seismic Pavement Analyzer (PSPA). PSPA can automatically conduct both IE and USW tests simultaneously and it is designed so that it would work on rough HMA surfaces.

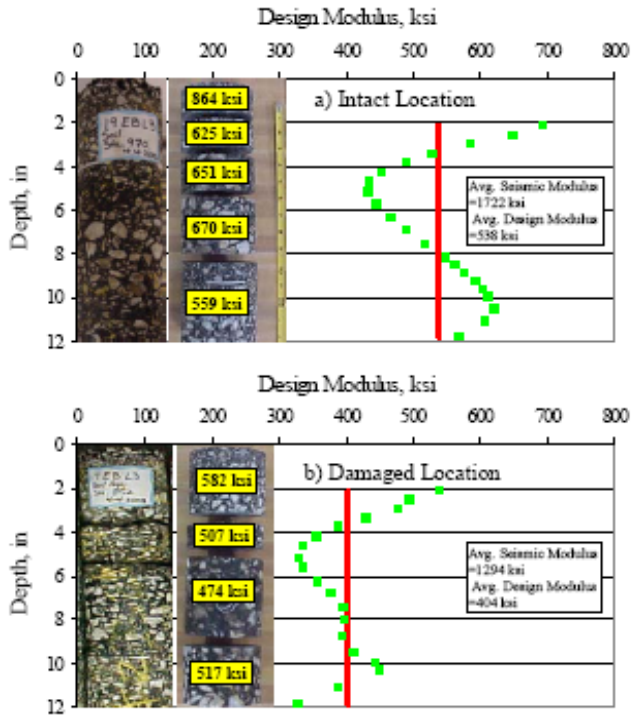


Figure 2.3: Typical Intact (Top) and Damage (Bottom) Dispersion Curves and Variation in Modulus with Depth for Cores.

The PSPA measures the average modulus of the exposed surface layers within a few seconds in the field. The PSPA, as shown in Figure 2.4, consists of two transducers (accelerometers in this case) and a source packaged into a hand-portable system, which can perform high-frequency (1 kHz to 50 kHz) seismic tests. The source package is also equipped with a transducer for consistency in triggering. The outputs of the three transducers from the final three impacts are saved and averaged for more reliability. These records are used to determine the velocity of propagation of waves in HMA layers.

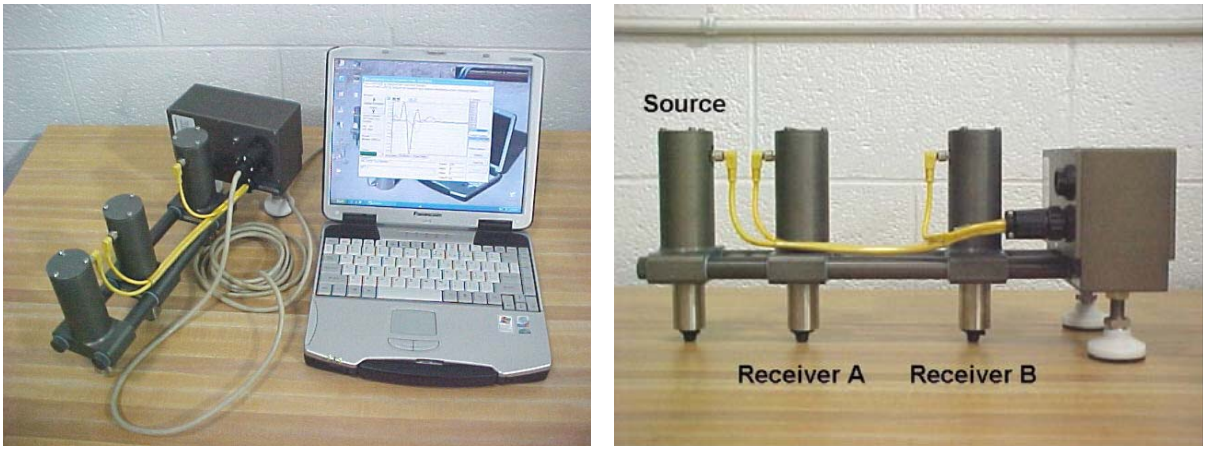


Figure 2.4: Portable Seismic Pavement Analyzer.

### 2.1.3 Impulse Response

Impulse-response method is a nondestructive technique that uses a low-strain impact to initiate stress wave propagation through the material investigated. The basic principle of the impulse response is to apply an impact to the surface tested and measure the vertical dynamic response using a velocity transducer or an accelerometer. The response to the impact is measured and analyzed to assess the in-situ condition. The instrument required for the impact is usually a 1-kg to 5-kg instrumented hammer. A typical set up of the method is shown in Figure 2.5.

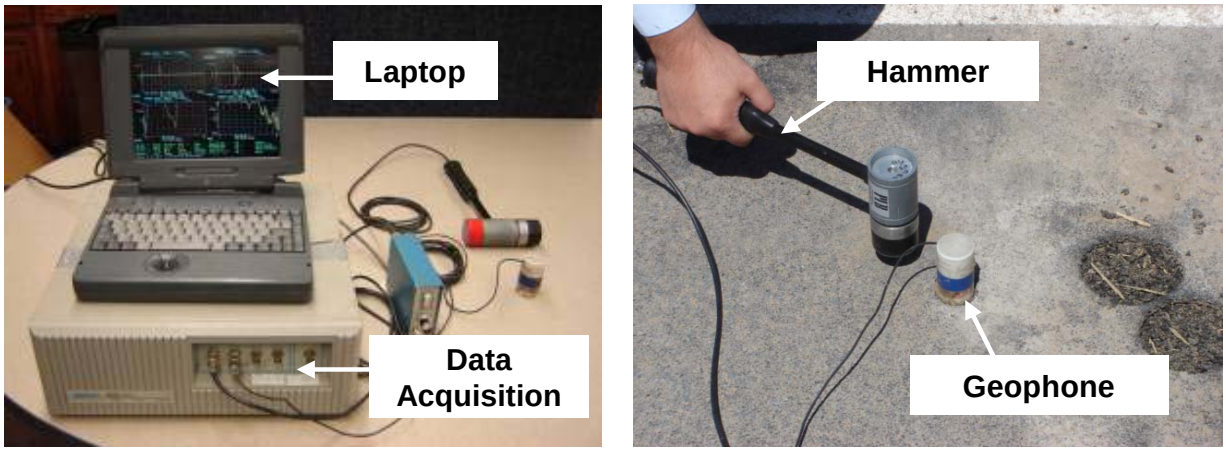


Figure 2.5: Typical Set Up of IR Method.

The elastic property of the hammer tip is related to the maximum compressive stress generated in the material by the impact. The stress levels can vary depending on the type of tip used for the impact, and it ranges from 5 MPa for hard rubber tips to more than 50 MPa for aluminum tips. For data acquisition both the hammer and the receiver are linked to a portable computer with the appropriate software. Once the data is obtained, the analysis can be completed in the field and typically includes the transfer function or mobility calculation by dividing the frequency spectrum of response by that of the input. The characteristics of the time history of the response as well as the shape of the graph of mobility plotted versus frequency contain information about the condition and the integrity of the material tested. An illustration of two mobility plots obtained on a sound and delaminated slab is shown in Figure 2.6.

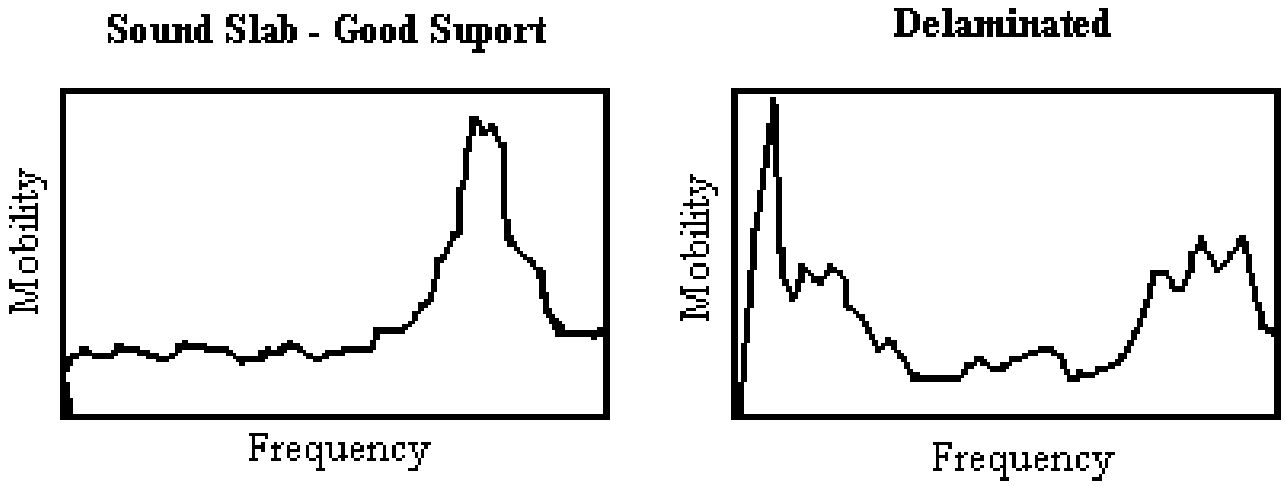


Figure 2.6: Example of IR Signals for Intact and Delaminated Slabs.

Kruntcheva et al. (2004) studied the feasibility of using the IR method for quantifying the bond condition within HMA layers under controlled laboratory conditions. The study consisted of the construction of a slab with different surface HMA thicknesses with three types of interface conditions such as: bonded; debonded; and partially bonded. For shallow interfaces a 2.3 kg impulse hammer was used, for deeper interfaces, a 3.3 kg was required, and thus increased the peak forces needed for the test. To ensure the repeatability of the results, several input-output time histories were recorded at each particular position of the accelerometer.

An illustration of the differences in dynamic responses for the debonded and bonded interfaces in that study is shown in Figure 2.7. When the impulse was applied to the bonded area the displacement time records were smooth and of low frequency. On the other hand a jagged vibration response for the debonded sections was observed. This effect could also be identified by the oscillatory components of the acceleration response, which were out of phase with respect to the excitation. The oscillatory behavior of the debonded section after the impact was evident for a predominant forced damped vibrations with much longer decay time in comparison with the ‘‘wave’’ response of the bonded section. For this reason, a prompt diagnostic of the condition of the interface of the section tested can be made by a visual inspection of the time histories.

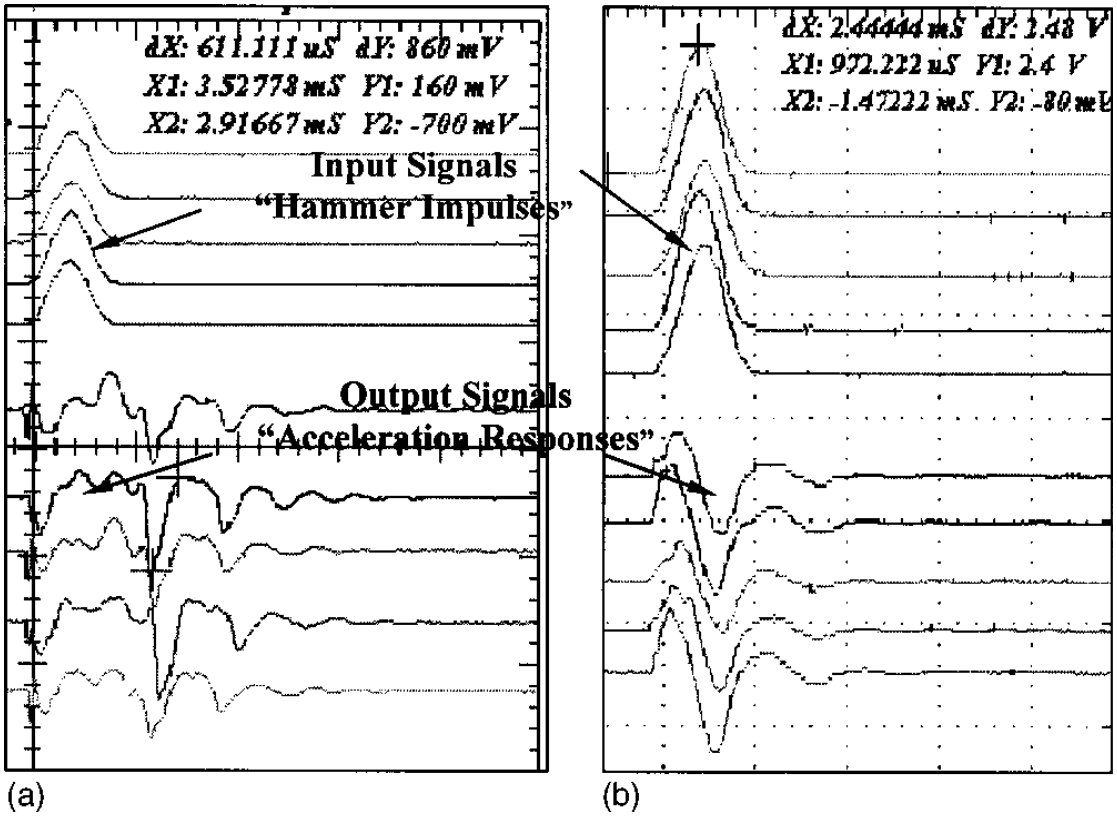


Figure 2.7: Time Histories of Input and Output Signals for Debonded (a) and Bonded (b) Surfacing (from Kruntcheva et al., 2004).

For the in-situ assessment of bond condition between surface and base courses for different types of surface course, the IR method was used in another study by Sangiorgi (2003). In that case, two sections with different materials and thicknesses were tested in two different seasons of the year. The materials used for the surface course were a proprietary surfacing known as "thinpave" and a standard 10 mm "close-graded Macadam" with a thickness of 20 mm and 30 mm, respectively. Moreover each section was divided into three sub-sections with different treatments for interface conditions to simulate different levels of bond condition at interfaces. The treatments were the application of a regular amount of tack coat, a swept surface with no tack coat and clay slurry at the interface.

Time histories acquired for the two cases of intact and debonded interfaces are shown in Figure 2.8. The results obtained were comparable to those obtained by Kruntcheva et al. For the debonded case the signal showed vibrations of higher frequency and the acceleration did not decrease to zero until approximately 6 ms. On the other hand, the signal obtained from the bonded section showed an acceleration of lower frequency decreasing to zero after 1.5ms.

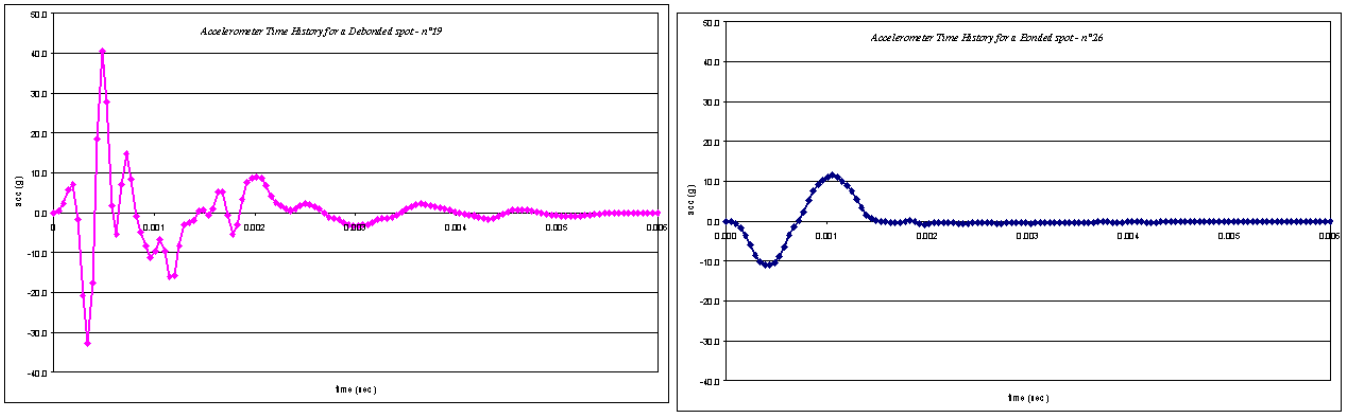


Figure 2.8: Typical Debonded (Left) and Bonded (Right) Time Histories (from Sangiorgi, 2003).

Based on the studies presented in previous section, the IR method seems to be a reliable tool of delamination between HMA layers. Results from the IR method can vary depending on the surfacing materials and thickness, and the conclusions cited by the studies mentioned above were based on controlled laboratory studies rather than field investigations.

## 2.2 FINITE ELEMENT METHOD

Several studies for the comprehensive evaluation of concrete bridge decks using impact echo have been previously conducted on two-dimensional (2D) finite element models (Shokouhi, 2006). Shokouhi considered a number of criteria to ensure the accuracy of the numerical result. The overall dimension of the model should be large enough to avoid the contamination of the signal by the compressive ways reflected from the artificial boundaries. The length chosen for the model was 2.5 m from the impact to the boundary and the thickness of the model was chosen as 0.25 m. The size of elements depended on the geometry of the model, the material property and on the impact loading function. A uniform element size of 5 mm was chosen for the model. The element size was chosen based on the highest frequency of interest and the minimum wavelength. The time step of 1 μs was small enough to prevent the compressive wave to "jump over" the smallest element in the model. The impact duration of 50μs was based on the characteristics of the impact sources used for the IE method. To avoid the contamination of the signal by compressive waves reflected from the boundaries the receiver was placed at a distance of 0.25 m from the impact. To set a material Rayleigh damping, a

stiffness damping $\beta=10^{-8}$ was used for the study. A "Clipping" technique was used to reduce the effects of the surface wave to the spectrum of the displacement, velocity and acceleration of histories.

Medina (2007) performed a finite element simulation focused on using advanced signal processing techniques to improve the analysis and facilitate the interpretation of IE test results, especially when low-frequency high-amplitude flexural vibrations may mask the resonant reflections of interest. The Rayleigh waves were removed by a "windowing" operation, and a multicross-spectral density function was defined by applying cross-spectral density to the signals collected at several distances from the impact point. This process eliminated several undesirable peaks contained in the frequency spectrum by applying the Blackman-Harris window over the recorded wave as shown in Figure 2.9, thus interpretation of the longitudinal waves becomes much easier.

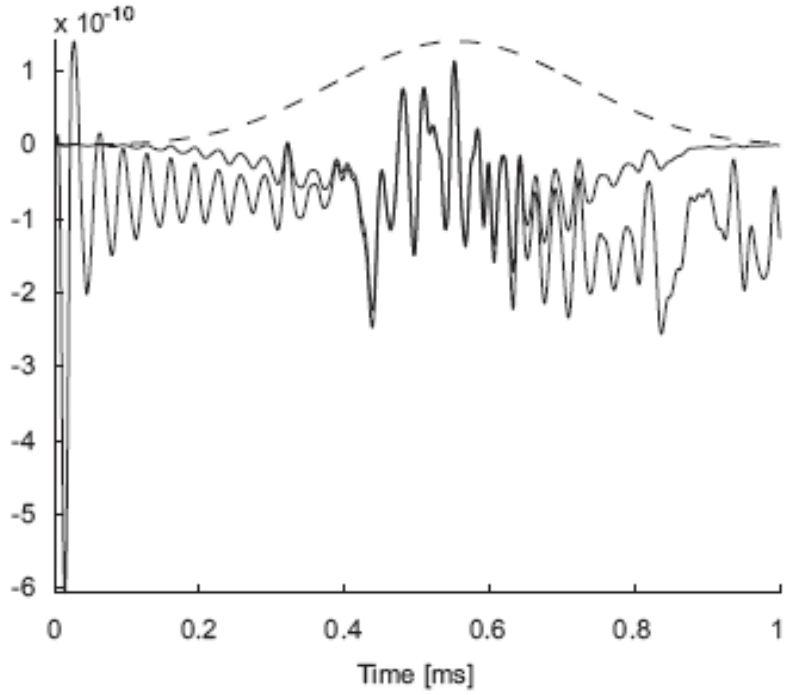


Figure 2.9: Blackman-Harris Window Applied to the Recorded Wave.

To validate the proposed method, Medina used a finite element model of composite (asphalt over concrete) thin plates with shallow debonding at the interface of the asphalt overlay placed on a concrete slab. The noise and the undesirable peaks in the frequency domain were reduced after the technique was applied, facilitating the interpretation of the results.

In one case study, a small plate made up of two layers was considered. The radius of the plate was 400 mm, and the top layer (asphalt) and the bottom concrete layer were 20 and 30 mm thick respectively. A shallow delamination in the contact zone between the concrete slab and the asphalt overlay was considered. The spectra from the raw and filtered signals are compared in Figure 2.10. In the IE spectrum, the resonant frequency of delamination was difficult to detect mainly because the amplitudes of the flexural modes of vibration of the thin asphalt layer were dominating the spectrum. When the low frequency peaks of the flexural modes were removed and the multicross-spectral density function was applied, only the peak corresponding to the delamination depth was evident, demonstrating the usefulness of the proposed method (Figure 2.10).

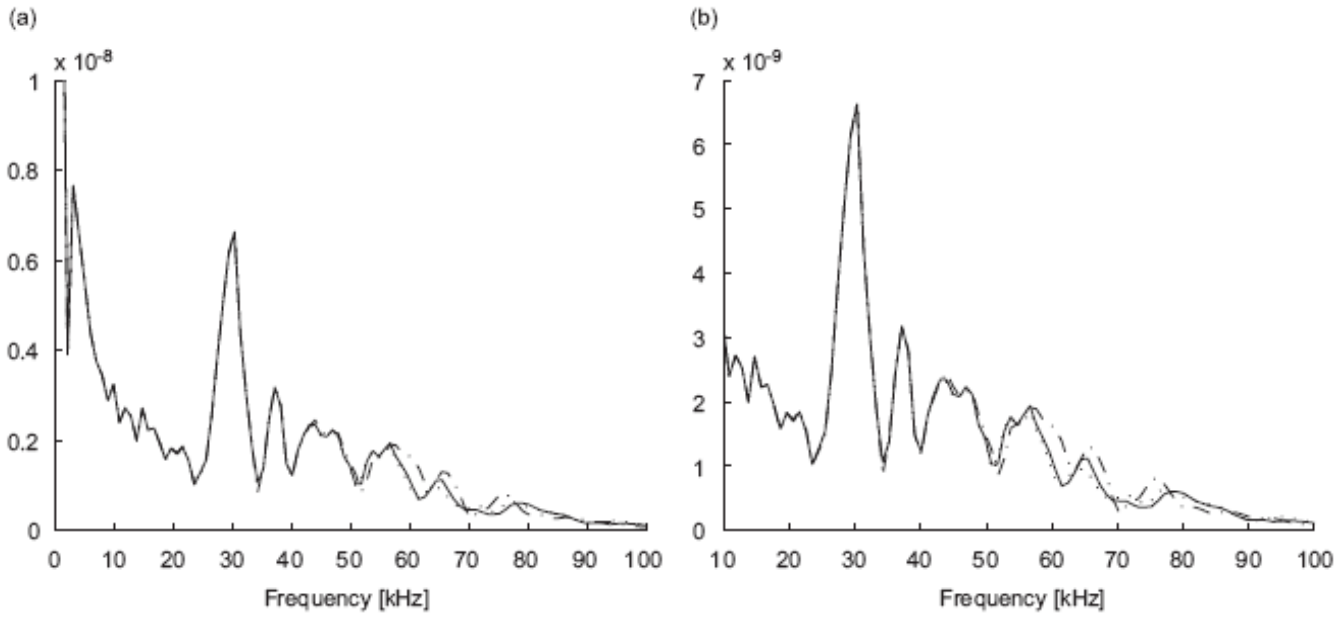


Figure 2.10: Comparison between Whole Signal and Filtered Signal.

# Chapter 3: Finite Element Method Set-up

Finite Element method (FEM) was used in this study to recreate the results obtained from IE, USW and IR methods when they are employed for the detection of delamination between HMA layers. In this numerical study, three-dimensional (3D) finite element models of intact and delaminated HMA pavements were developed. The software used to perform the analysis was LS-DYNA. LS-DYNA is a general purpose multiphysics transient dynamic finite element program capable of simulating complex problems that is actively developed by the Livermore Software Technology Corporation.

For the numerical study a number of criteria have been taken into account to ensure the accuracy of the results. A description of the finite element models and the requirement criteria will be presented in the following sections. The criteria considered for the numerical analysis are the dimensions of the model, element size, time step and duration of the impact.

## 3.1 EXPERIMENTAL SET-UP

The dimensions selected for the IE and USW models were 0.50 m by 0.50 m (length and width) with a depth of 0.50 m. Non-reflecting boundaries were applied to the model to avoid the contamination of the signal due to the reflection of stress waves from the boundaries. The model was divided into seven different layers. The layers were placed from top to bottom in the following manner: four layers with a depth of 0.05 m each for the HMA layers, then two layers with a depth of 0.10 m to represent the base course and one layer with a depth of 0.10 m. for the subgrade as shown in Figure 3.1. A non reflecting boundary was applied along the bottom to simulate the continuity of the subgrade.

For the IR models, the dimensions of 2 m by 2 m (length and width) with a depth of 0.50 m were selected for the pavement section as illustrated in Figure 3.2. The same criteria of non-reflecting boundaries and layered system from the IE models were used for the IR models.

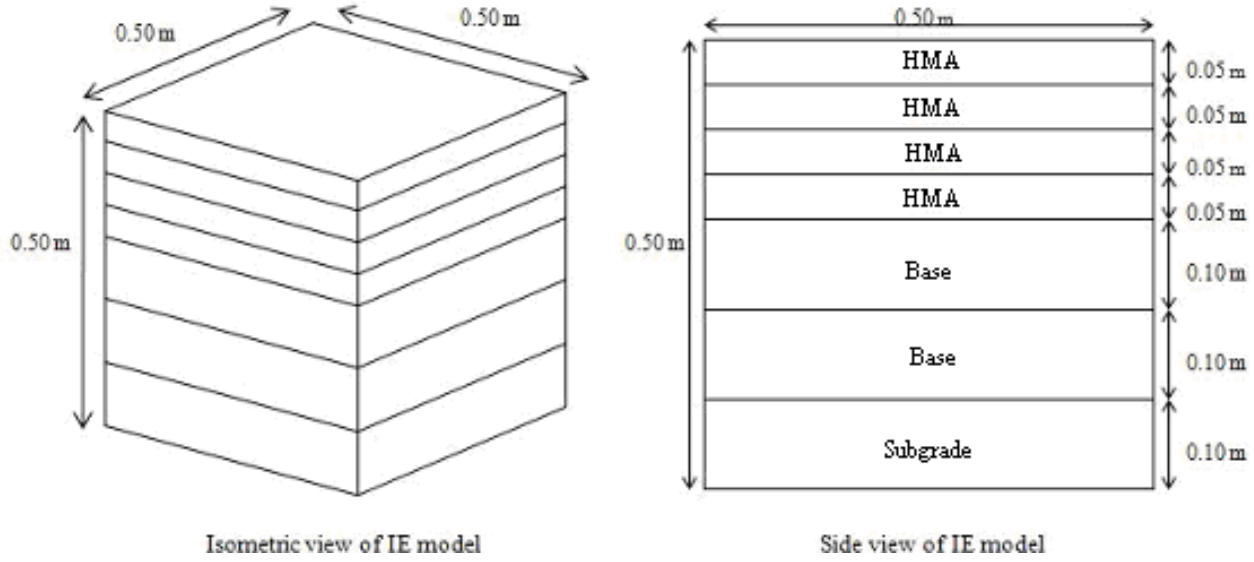


Figure 3.1: Impact Echo Custom Model.

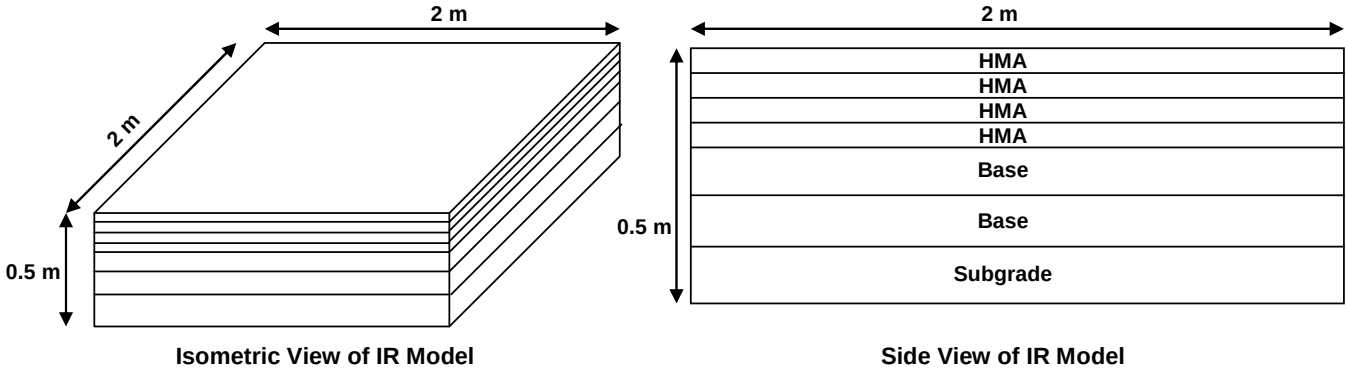


Figure 3.2: Impulse Response Custom Model.

It is very important to select the correct size of elements. Very large elements will filter high frequencies while very small elements can generate numerical instability as well as require too much computational resources. Element size depends on the shortest wavelength ($\lambda_{min}$) along the direction of wave propagation. A relation to obtain the shortest wavelength is given by the following equation (Zerwer, 2002):

$$\lambda_{\min} = \frac{C_c}{f_{\max}} \tag{3.1}$$

where, the velocity of propagation, *Cc*, is determined from:

$$C_c = \sqrt{\frac{E}{\rho}} \tag{3.2}$$

and

$$f_{\max} = \frac{C_c}{2h} \tag{3.3}$$

Assuming a modulus of elasticity (E) of 12.5 GPa, density (□) of 2150 kg/m3, and minimum thickness (h) of 0.05 m, □min of 0.1 m was obtained. Based on these results an element size of 0.01 m was selected for the IE model which is less than the shortest wavelength and it is not too small to cause numerical instability. Expecting lower frequencies for the IR and based on the same principle for IE, an element size of 0.025 m was selected. The element type was 8-nodes hexahedron solid element for both models.

The time increment at which the time-displacement waveform has to be calculated has to be small enough to prevent the compressive wave to "jump over" the elements in the model on the other hand if the time increment is too small it will result in oscillations (Gibb's phenomenon) in the time-displacement waveform record. The time increment, $\Delta t$, can be obtained using the following formula:

$$\Delta t = \frac{1}{2 f_{\max}} \tag{3.4}$$

This sampling frequency has to satisfy the effective length ($l_e$) of the model which corresponds to the element size. Following the Bathe (1996) criterion, the time increment ($\Delta t$) should be less than:

$$\Delta t \leq \frac{l_e}{C_c} \tag{3.5}$$

For the le of 0.01 m used in the IE and USW model, a $\Delta$t of 1.85μs was chosen, which satisfies the criteria mentioned, and do not require excessive time for computational calculations. For the IR models, a $\Delta$t = 0.1 ms was chosen taking into account that elements for IR models are greater than those for the IE models. Shorter time increments introduced numerical instability.

Impact duration depends on the characteristics of the impact sources commonly used for both the IE/USW and IR techniques. The pulse of the impact can be defined as a half-sine curve, and the duration of the impact is related to the size of the impactor. In this study, a hamming curve was used to simulate the impact for both the IE and IR models. Impact durations of 52.5 μsec and 0.2 ms were chosen for the IE/USW and IR models, respectively. Since a linear-elastic model was used, the

magnitude of the impulse load is irrelevant. The maximum load of 5N and 27500 N for IE/USW and IR respectively were chosen, the load was applied in 21 load steps in all cases. An illustration of the impact for IE/USW and IR are shown in Figure 3.3.

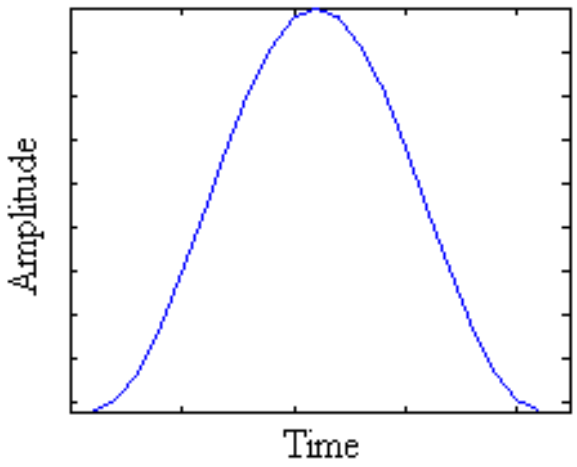


Figure 3.3: Hamming Curve for the Simulation of the Pulse Impact.

For IE/USW the impact was applied as a point load at the center of the top edge of the top layer and for the IE a receiver was placed at 0.05 m from the impact (Figure 3.4a) therefore the acceleration of the node at that distance was taken. For the USW the measurement of the acceleration was taken at three different nodes, at the impact and at 50 and 100 mm away from the impact. An illustration of the set-up is shown in Figure 3.4b.

A time record of 1.5 ms was selected to ensure enough data for the analysis. In the case of IR the impact was applied over an area of 50 by 50 mm which correspond to the area of the hammer tip and the receiver (geophone) was place it at a distance of 50 mm away from the edge of the area impacted (Figure 3.4c) and it measured the velocity of the wave at that point.

The interface between different layers was modeled as debonded, partially-bonded or fully-debonded. To simulate total bonding between layers the command contact with the option of "*tied surfaces*" was selected. With this option two different layers act as one allowing P-waves travel trough the layers without reflecting at the interface.

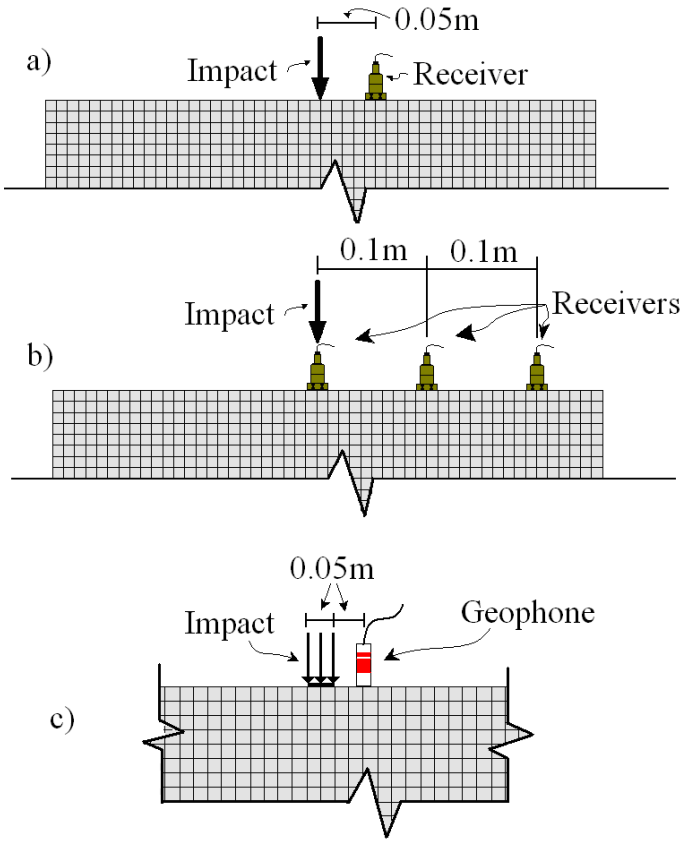


Figure 3.4: Schematic of Set-up for a) IE, b) USW and c) IR.

To simulate the total debonding the command contact with the option "*surface to surface*" from LS-DYNA was selected. This option permitted to have two layers without bonding at the interface. Therefore the P-waves were totally reflected at the interface.

To simulate partial debonding the command contact with the option "*sliding only*" was employed. This option allowed the condition to have enough separation between layers to reflect the P-waves and enough bonding to the transition of the P-waves to the other layers. This is because at the interface there are just shear stresses originating reflections at both sides.

To apply contact between different layers it is necessary to use segments which will have the attributes of the type of contact required and as a result an interface condition between layers. For a given model a single segment was used to establish an interface condition between the subgrade and the base, as well as, for the base and HMA layer. To establish an interface condition between HMA layers an arrangement of segments of different shapes was provided to create the size of defect required. The arrangement of segments for IE/USW and IR are shown in Figures 3.5a and 3.5b.

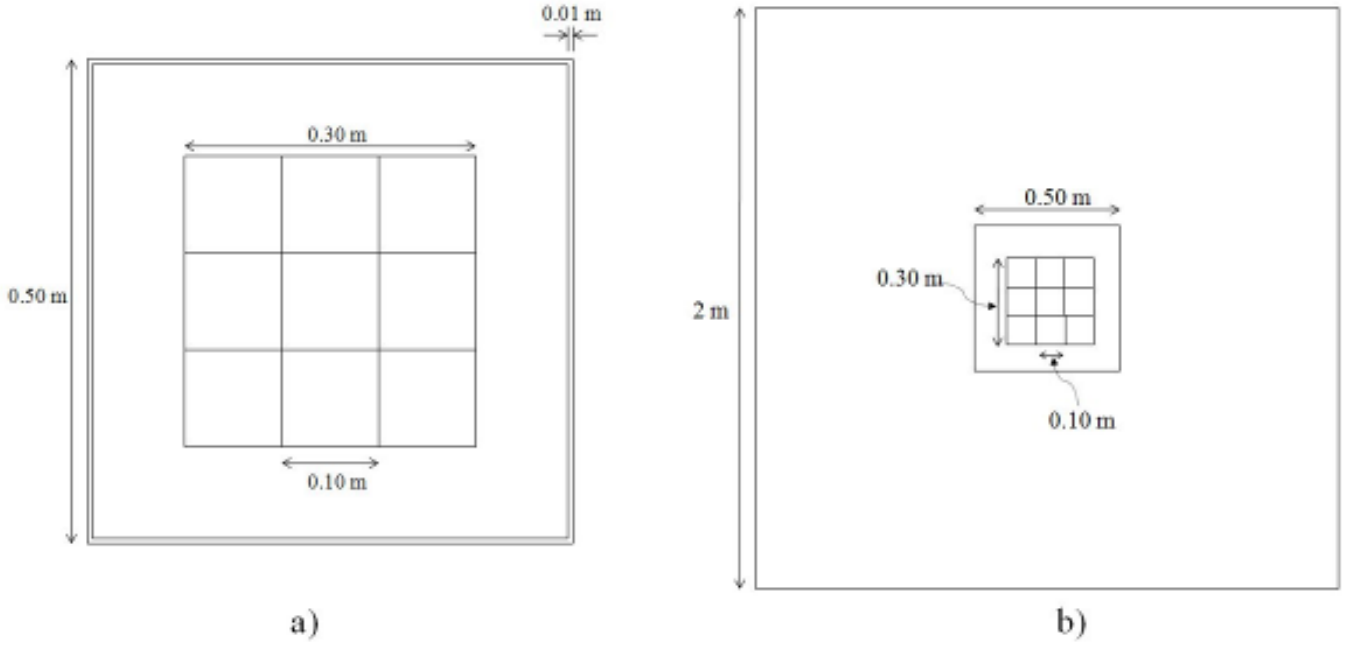


Figure 3.5: Application of Contact to Establish an Interface Condition by Using Segments, a) Arrangement of Segments between HMA Layers, b) Arrangement of Segments for IE/USW, c) Arrangement of Segments for IR.

For example Figure 3.6 shows the schematic to create different sizes of delamination for the model selected for IE/USW. A similar approach was followed for the IR models. To create a bonded interface condition between layers, all the segments had the contact option of "*tied surfaces*" (Figure 3.6a). To induce a delamination, a number of segments to satisfy the dimension of the delamination were selected. Then the contact option of "*surface to surface*" or "*sliding only*" was activated to create a total debonded or partial debonded interface condition, respectively. The contact option of "*tied node*" was activated for the remained segments. By using this procedure a large amount of combinations could be achieved for different sizes of delamination. As an example, Figures 3.6b, 3.6c and 3.6d, show delaminations of 0.1 by 0.1, 0.3 by 0.3 and 0.5 by 0.5m respectively for the IE/USW model.

Material damping was included in the form of stiffness damping to reduce high frequency oscillations without significantly altering the overall force-strain performance. After performing a series of analyses of wave propagation on the model with varying values of the coefficient of stiffness β and comparing the attenuation levels to those from available field records, β= 0.00016 and β= 0.001 were chosen for IE/USW and IR, respectively.

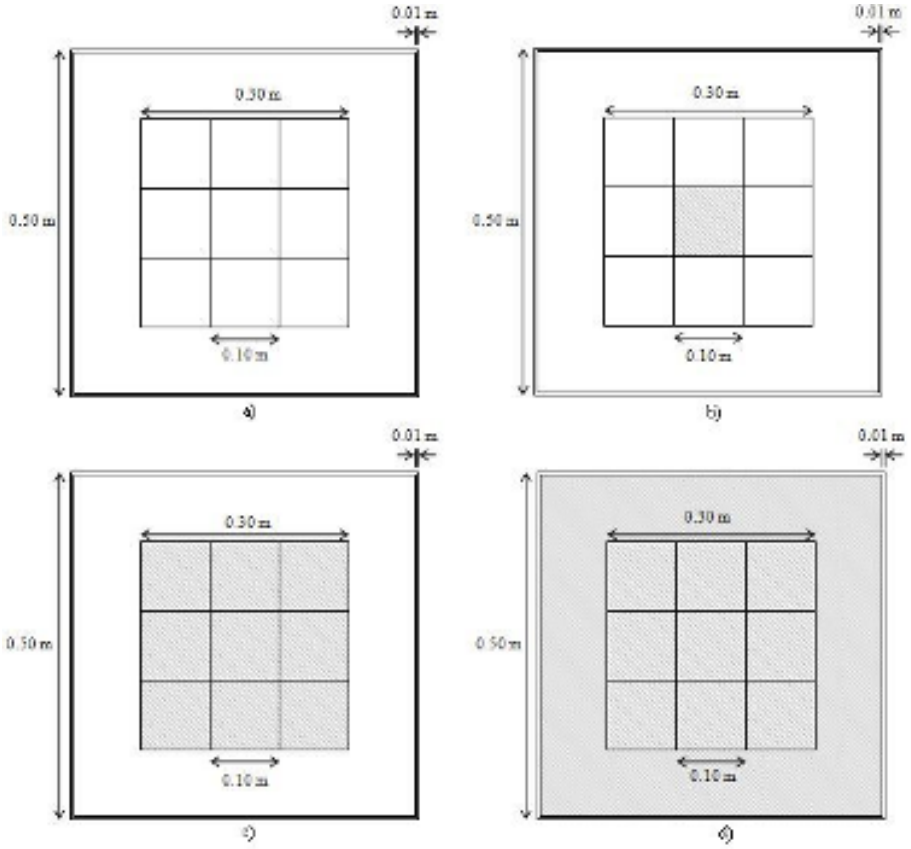


Figure 3.6: Arrangement of Segments between HMA Layers; White Segments Correspond to Bonded sections, and Shadowed Segments Correspond to delaminated sections. a) Intact Interface Condition, b) Defect of 0.1x0.1m. c) Defect of 0.3x0.3m., d) Defect of 0.5x0.5m.

To process the IE data, an algorithm in MATLAB was developed. A Blackman-Harris window (Figure 3.7) was applied to the time-domain signal to highlight the P-waves. The filtered data were then transformed into the frequency domain by using fast Fourier transform (FFT). Figure 3.8 summarizes theses steps.

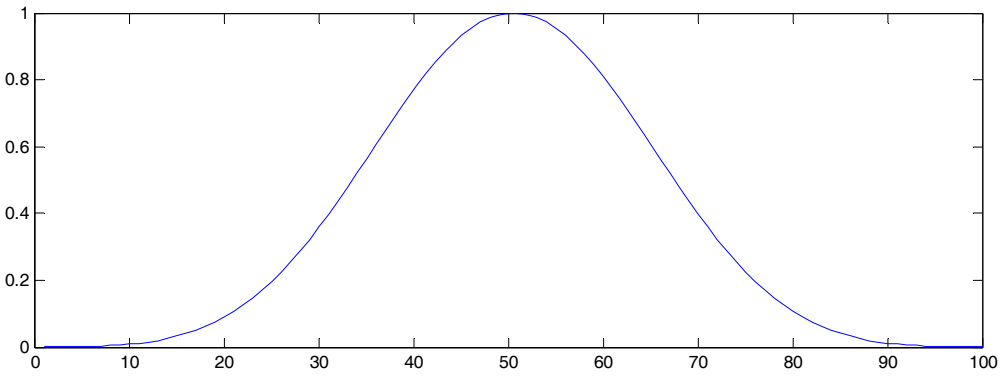


Figure 3.7: Blackman-Harris Window.

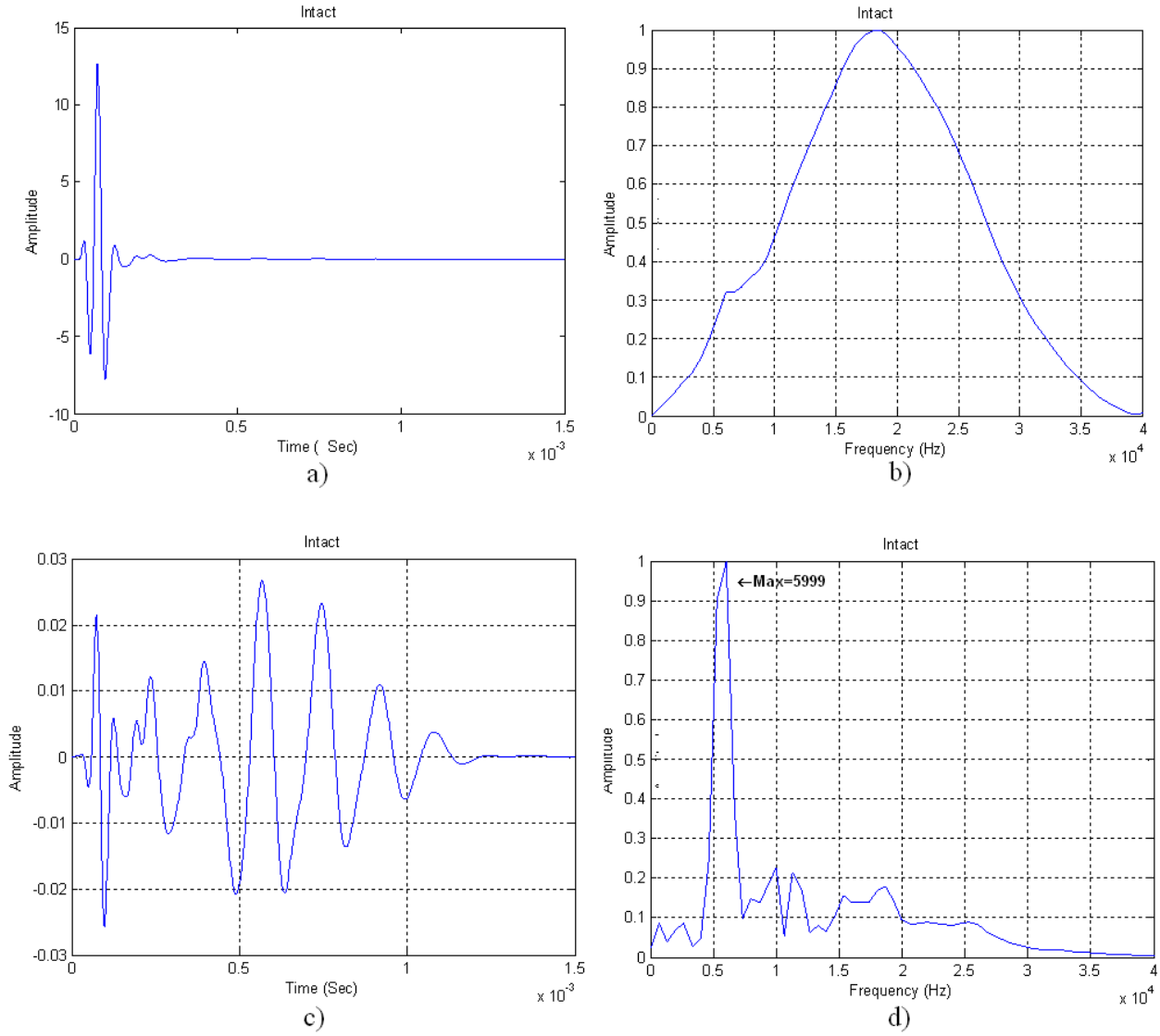


Figure 3.8: Difference of Frequency Spectrum using the Blackman-Harris Window.

Same data was then analyzed using the USW method. A software developed at the University of Texas at El Paso named CPSPA was used to obtain the dispersion curves of the models from the data acquired from two sensors. Different steps for this action are shown in Figure 3.9.

For IR method, the time domain signals corresponding to the input load and the response from the receiver were transformed into the frequency domain with an FFT algorithm. The ratio of the maximum amplitudes from the load and velocity was calculated as an indicator of debonding or delamination. The steps for this process are shown in Figure 3.10.

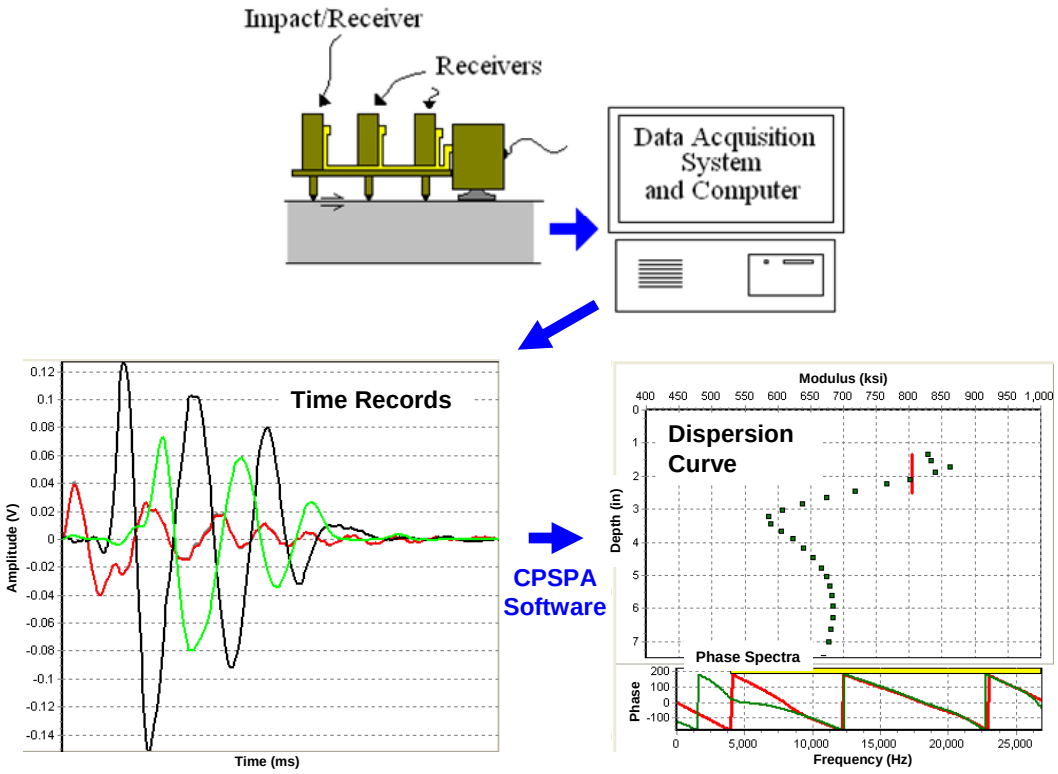


Figure 3.9: Diagram of the USW Method.

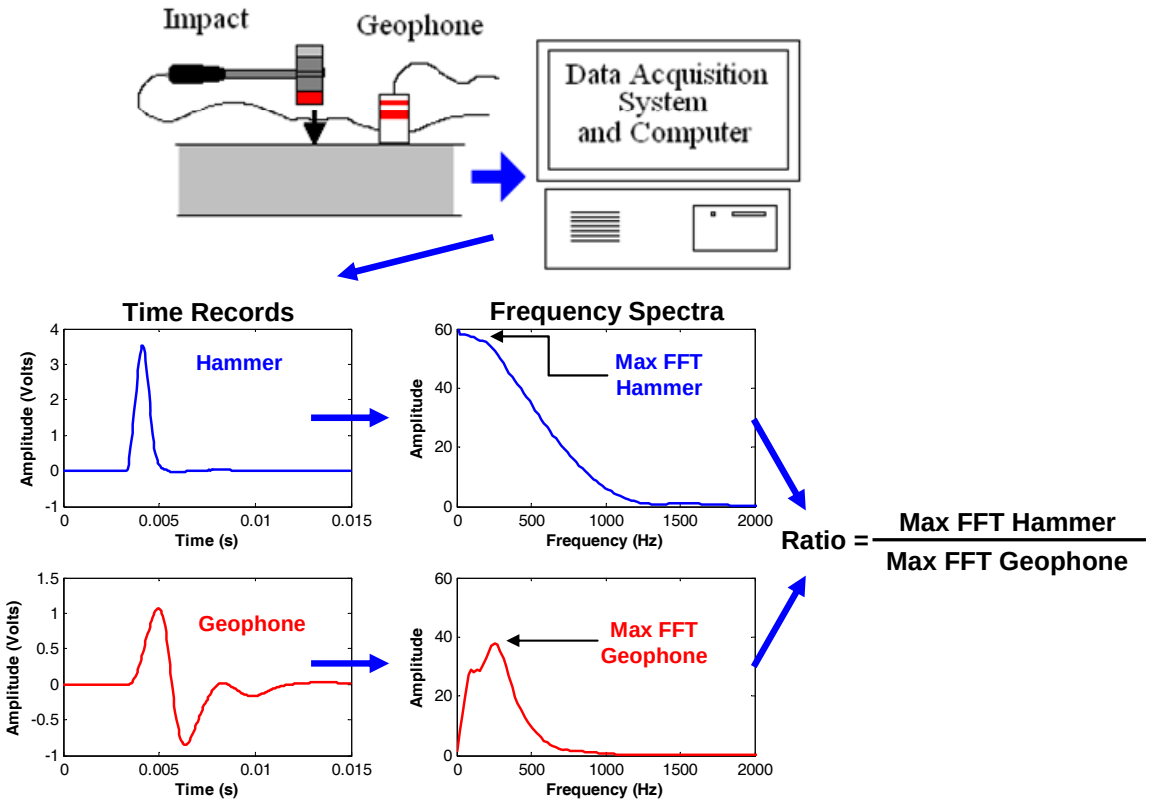


Figure 3.10: Diagram of the Impulse Response Method.

## 3.2 PARAMETRIC STUDY SET-UP

Once the models for IE, USW and IR were defined, a parametric study was carried out. The parameters considered were the properties of the flexible pavement such as modulus, Poisson's ratio and layer thickness. Other parameters considered were the interface conditions such as, total bonding, partial bonding and total debonding between layers, as well as, the size and depth of defect. Taking this into account, properties for a typical pavement section were established. Those properties for a control pavement model are shown in Table 3.1. The parameters considered in the parametric study are summarized in Table 3.2.

Table 3.1: Properties of the Flexible Pavement Section for the Control Model.

| Material | Density (kg/m3) | Modulus of Elasticity (MPa) | Poisson's Ratio | P-wave Velocity (m/s) | Layer thickness (m) | Depth of Defect (m) | Size of Defect (m) |
|---|---|---|---|---|---|---|---|
| HMA | 2150 | 12500 | 0.33 | 2411 | 0.20 | 0.10 | 0.50 |
| Base | 2100 | 700 | 0.35 | 577 | 0.20 | 0.10 | 0.50 |
| Subgrade | 2000 | 137 | 0.35 | 261 | infinite | 0.10 | 0.50 |

Table 3.2: Parameters from the Flexible Pavement.

| Variable | Level | Description |
|---|---|---|
| Interface Condition | 3 | Bonded, Partially Bonded, Debonded |
| Depth of Defect | 3 | 50 mm, 100 mm, 150 mm |
| Size of Defect | 3 | 100x100 mm, 300x300 mm, 500x500 mm |
| HMA Modulus of Elasticity | 4 | 12.5, 8.3, 6.25 and 4.2 GPa |
| Base Modulus of Elasticity | 3 | 1250, 700 and 315 MPa |
| HMA Thickness | 3 | 200 mm, 150 mm and 100 mm |

# Chapter 4: Evaluation of Results

Depending on the method, the technique used to compare the results was different. For the IE method, first a comparison between waveforms (normal and windowed signals) was made, and then an evaluation of the corresponding frequency spectra was carried out. For the USW method, the dispersion curves obtained from the waveforms of every case were used. Finally, for the IR method, the time records were plotted and then comparisons of the ratio of the maximum velocity and maximum load were carried out.

It is important to mention that for all comparisons the properties of the pavement, the dimension and depth of the defect, that were used were those from the control model, and depending on the evaluation, those parameters remained equal. For instance, to evaluate the impact of interface condition the only parameter changed was the type of contact, while other properties remained constant, as previously described in Table 3.1.

## 4.1 IE Evaluation of Results

The impact of the interface condition on the results from the IE method is shown in Figure 4.1. Typical time records from intact, debonded and partial-debonded interfaces, as shown in Figure 4.1a. Properties of the control model for the overall pavement section as previously described in Table 3.1 were used. Time records are similar except for the low amplitude steady-state signals that are more apparent for the debonded and partially-debonded records.

To clarify the interpretation of the raw signals, the Blackman-Harris window was applied. As shown in Figure 4.1b the filtered data shows the impact of the bonding more clearly. For the intact record, after an erratic initial signal the record exhibits a steady-state response. The record from the partially bonded section, however, exhibits two steady-state signals superimposed. The record for the debonded section exhibits a steady-state response as well but at much shorter period than the intact section.

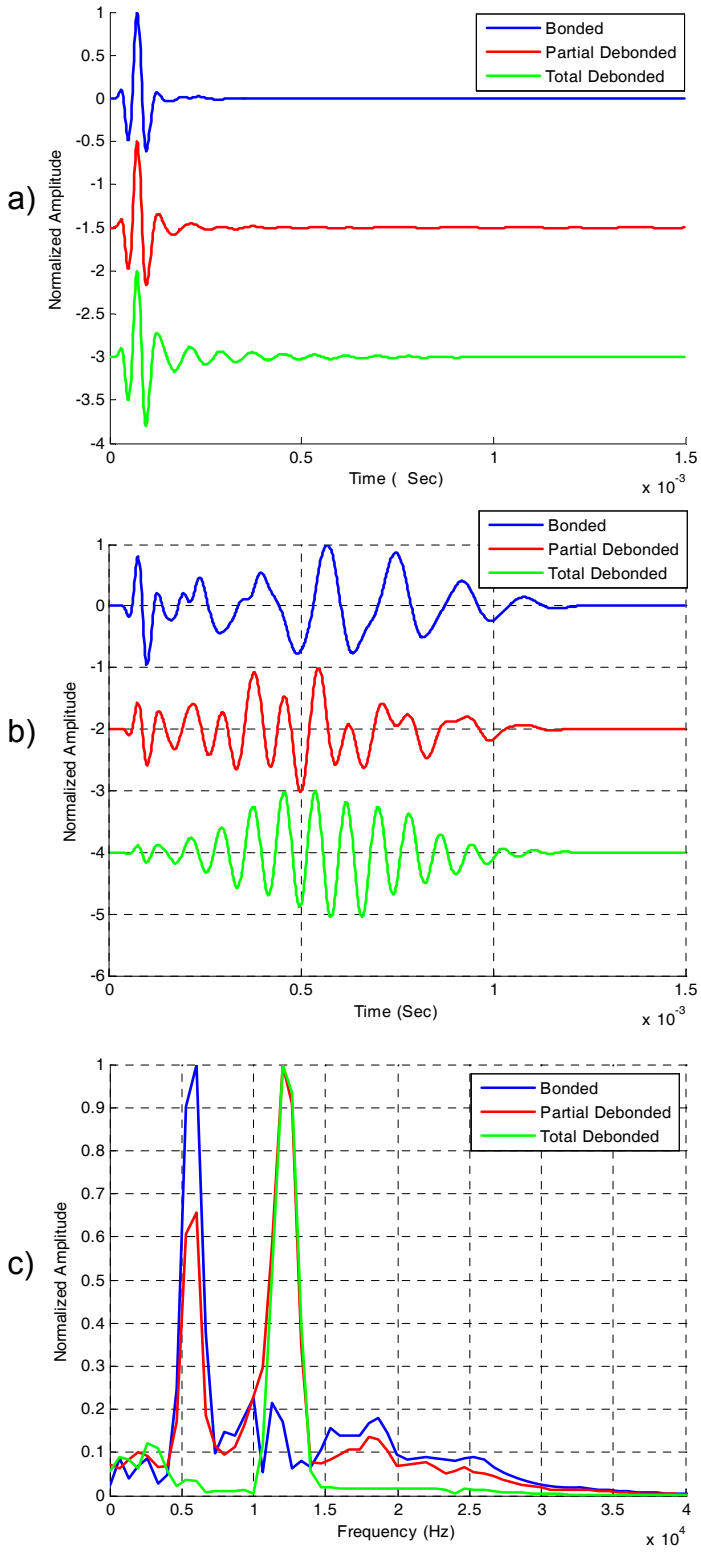


Figure 4.1: Impact of Interface Condition, Comparison of: a) Time Record Signals, b) Time Record after Applying the Blackman-Harris Window, c) Frequency Spectra of Signals.

The amplitude spectra of the same time records are shown in Figure 4.1c. For the intact section, a single peak appears at a frequency of about 6 kHz, which corresponds to the bottom of the HMA layer. The spectrum related to partial debonded section contains two peaks; the dominant peak has a frequency of 12 kHz which corresponds to the depth of defect, with a secondary peak at a frequency of 6 kHz which corresponds to the bottom of the HMA layer. This pattern was anticipated because most of the energy is reflected by the defect but some of that energy passes through the defect until it reaches the bottom edge and then it reflects. For the debonded section, the spectrum showed a single peak at a frequency of 12 kHz which corresponds to the defect. This indicates that there was a total reflection at the defect.

The impact of the depth of defect is shown in Figure 4.2. The depth of the defect was varied between 50 mm and 150 mm for the 200 mm thick HMA. The size of the defect to conduct this comparison was selected as 0.50x0.50 m for a total debonded model. Time records for the 100 mm and 150 mm deep defects after filtering show similar patterns. However, for the 50 mm deep defect, a large amplitude non-steady state response is apparent which corresponds to the flexural mode of vibration of the plate. As shown in Figure 4.2c, the deeper the defect is, the smaller the dominant frequency becomes, except for the 50 mm defect where the dominant frequency is about 2 kHz, attributed to the flexural mode.

The impact of the size of the defect for the IE method is shown in Figure 4.3. Sizes of 0.10 by 0.10 m, 0.30 by 0.30m, and 0.50 by 0.50m were evaluated. The depth of the defect was at 100 mm for the case of total debonding. The amplitude spectra of the 0.30x0.30 m and 0.50x0.50 m defects are very similar with the dominant frequency corresponding to the depth of debonding. This indicates that for defects larger than 0.30 m the IE method should be able to detect the debonding. On the other hand two dominant frequencies are observed for the 0.10x0.10 m size debonding. The more dominant frequency of slightly less than 6 kHz corresponds to the thickness of the slab. This dominant frequency is slightly lower than that from the intact slab because of the slightly longer distance that the wave has to travel to

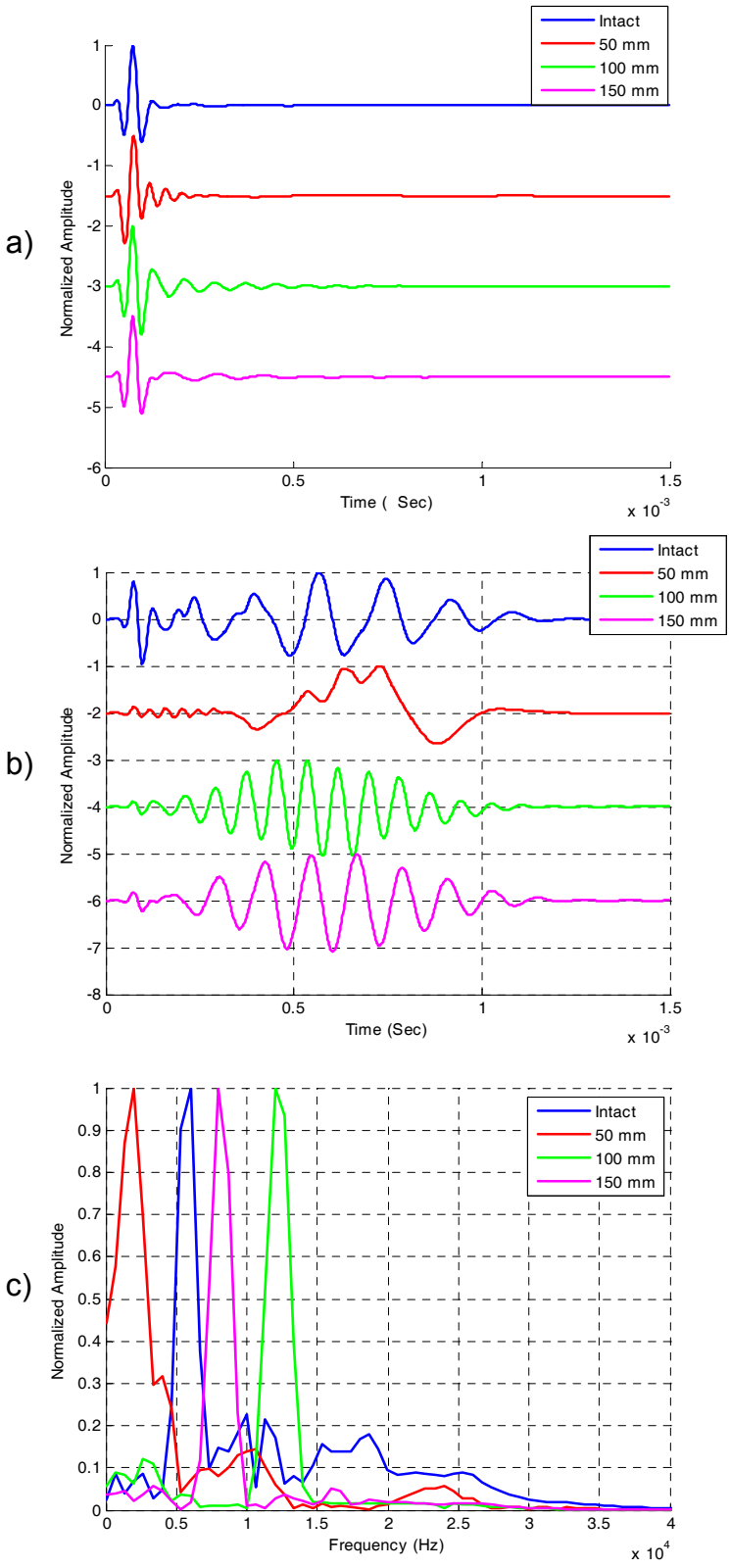


Figure 4.2: Impact of Depth of Defect, Comparison of: a) Time Record Signals, b) Time Record after Applying the Blackman-Harris Window, c) Frequency Spectra of Signals.

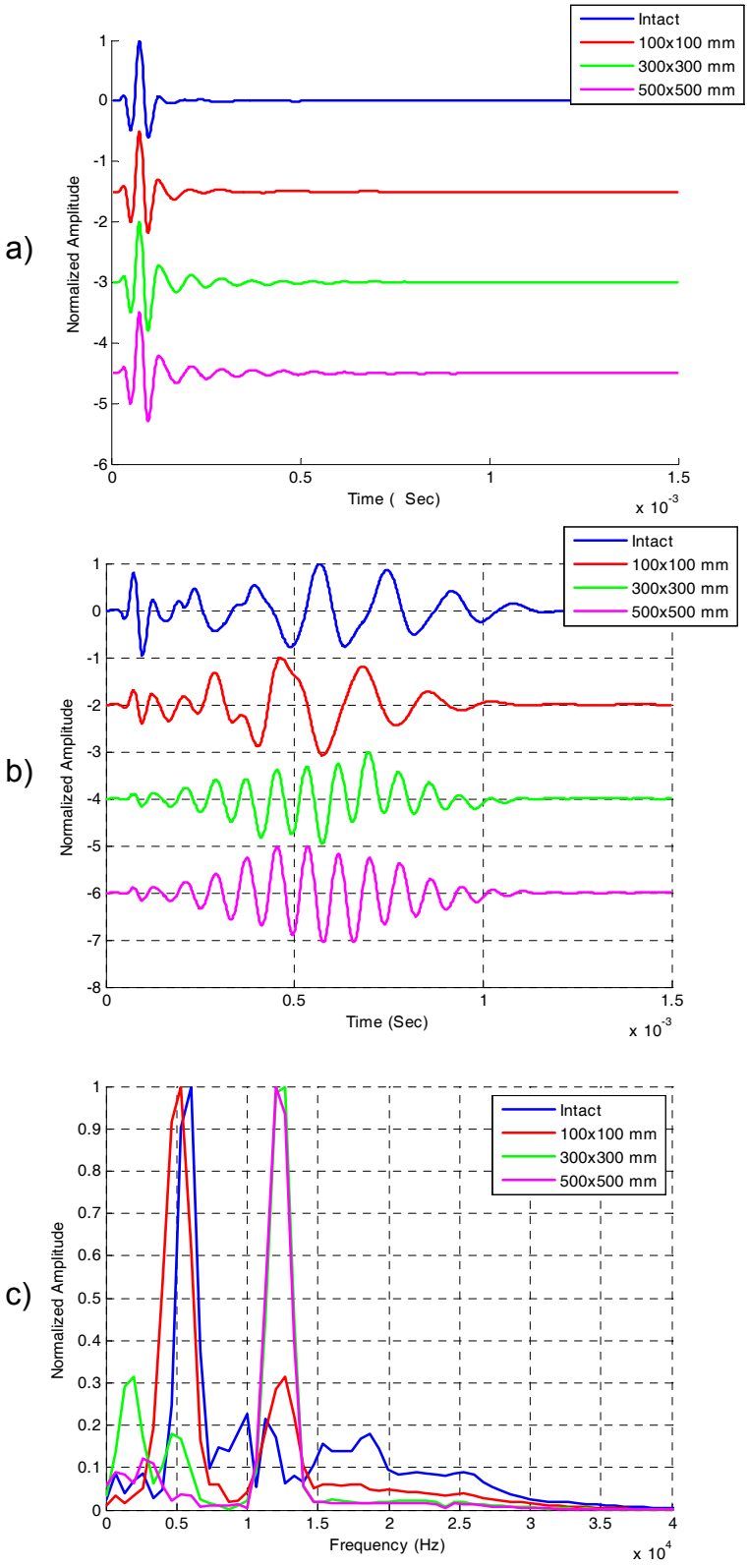


Figure 4.3: Impact of Size of Defect, Comparison of: a) Time Record Signals, b) Time Record after Applying the Blackman-Harris Window, c) Frequency Spectra of Signals.

reach to the bottom of the HMA. This wave had to propagate to the edge of the defect before propagating to the bottom of the HMA. The second dominant frequency, which occurs at about 12 kHz, corresponds to the reflection from the debonded interface. This frequency is absent from the intact section.

To consider the viscoelastic behavior of the HMA, the modulus of that layer was also varied. The results are presented in Figure 4.4. A defect of 0.50 by 0.50 at a depth of 100mm and total debonding between HMA layers were used. As the modulus of the HMA decreases, the dominant periods in time records become longer. As a result, the dominant frequency decreases. The significance of this data is that if the IE method has to be used for the detection of the delamination, the impact of the change in modulus should also be considered. This indicates that the modulus should be measured independently at each point.

As shown in Figure 4.5, the modulus of typical granular base does not seem to impact the results from the IE method. As indicated above, a total debonded defect of 0.50 by 0.50 at a depth of 100mm and was used. Three cases are presented with different modulus for the base: 300 MPa, 700 MPa (control) and 1250 MPa. Similarly, the thickness of the HMA layer does not seem to impact the detection of the debonding either (see Figure 4.6). A total debonded model and asphalt thicknesses varying from 10 to 20 mm were used. It can be observed that dominant frequencies for all spectra are quite similar.

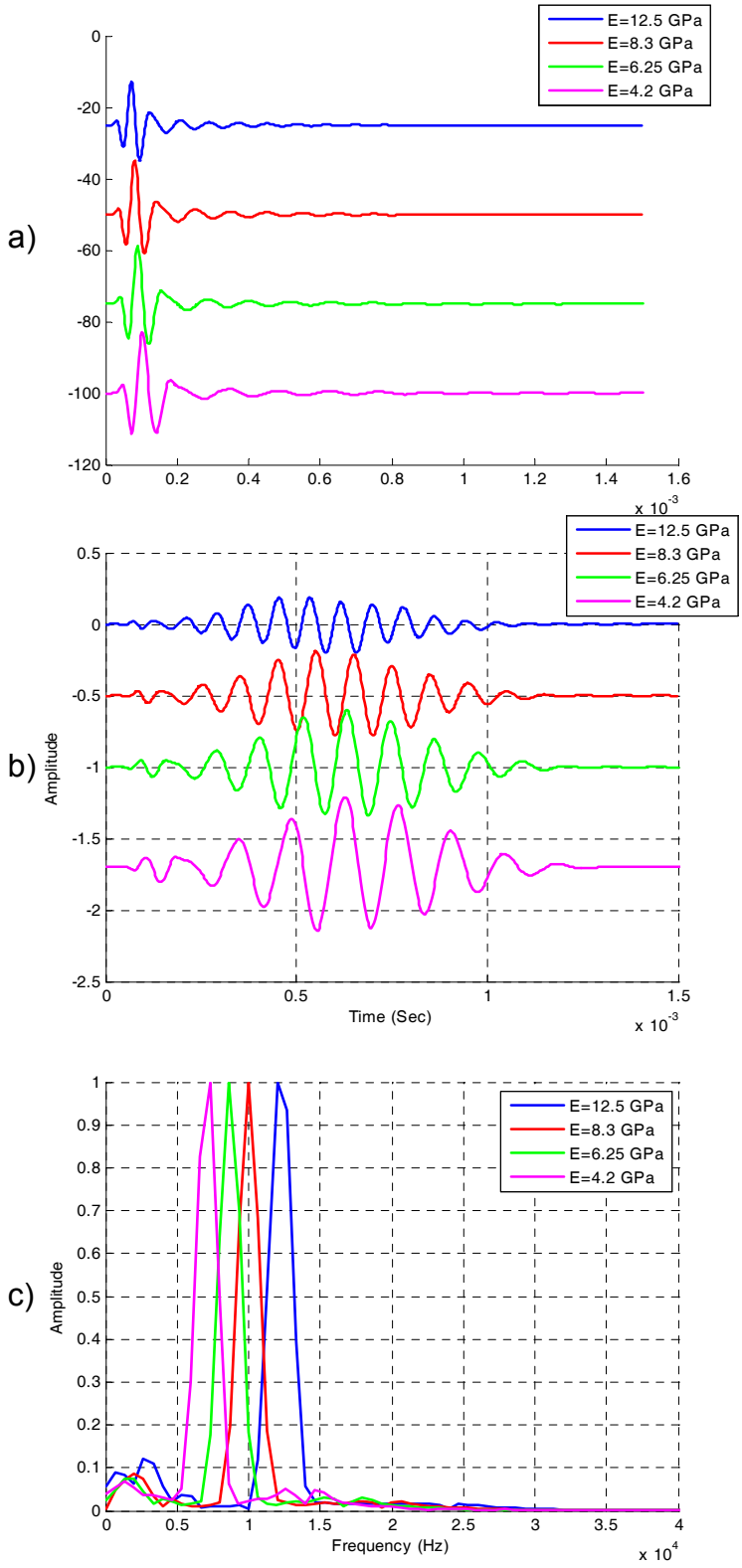


Figure 4.4: Impact of Modulus of Elasticity of HMA, Comparison of: a) Time Record Signals, b) Time Record after Applying the Blackman-Harris Window, c) Frequency Spectra of Signals.

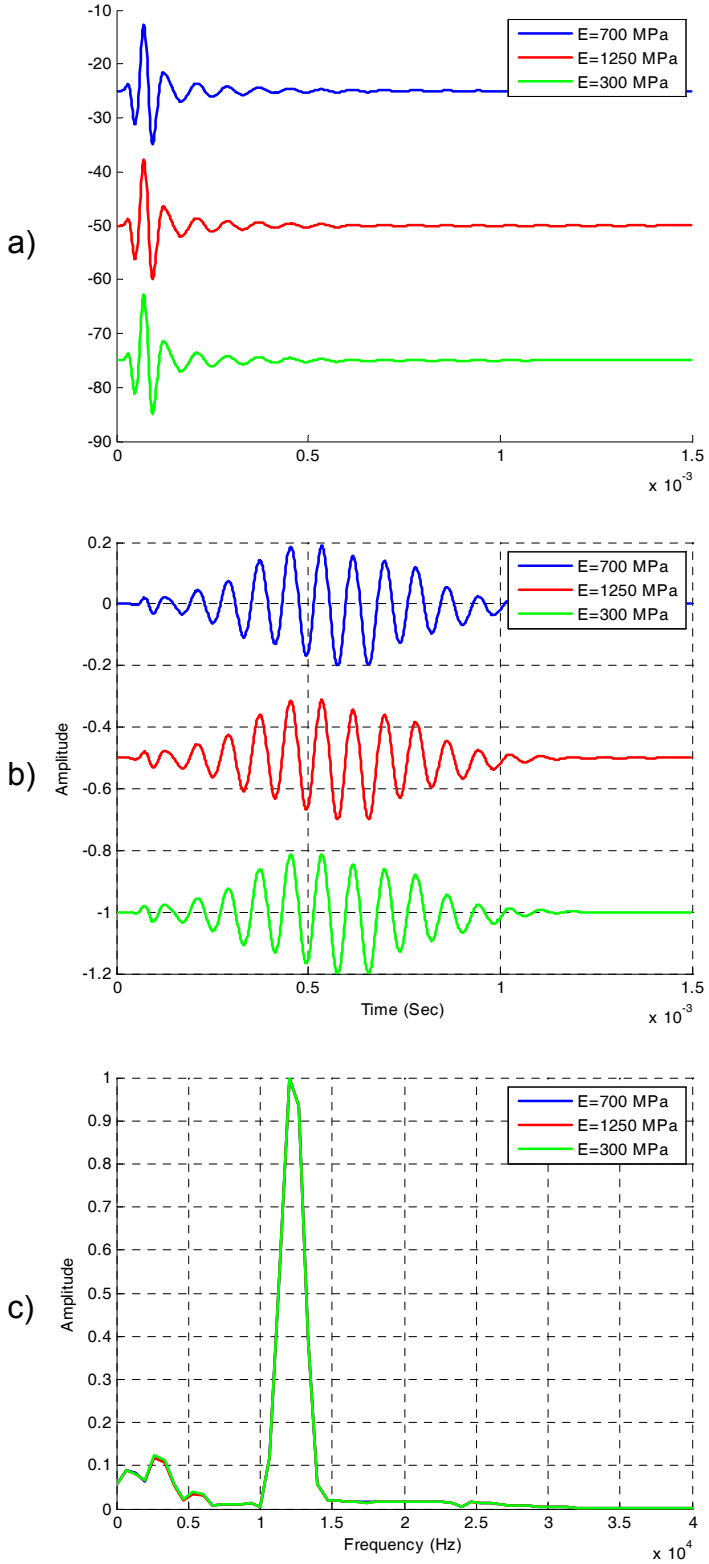


Figure 4.5: Impact of Modulus of Elasticity of Base, Comparison of: a) Time Record Signals, b) Time Record after Applying the Blackman-Harris Window, c) Frequency Spectra of Signals.

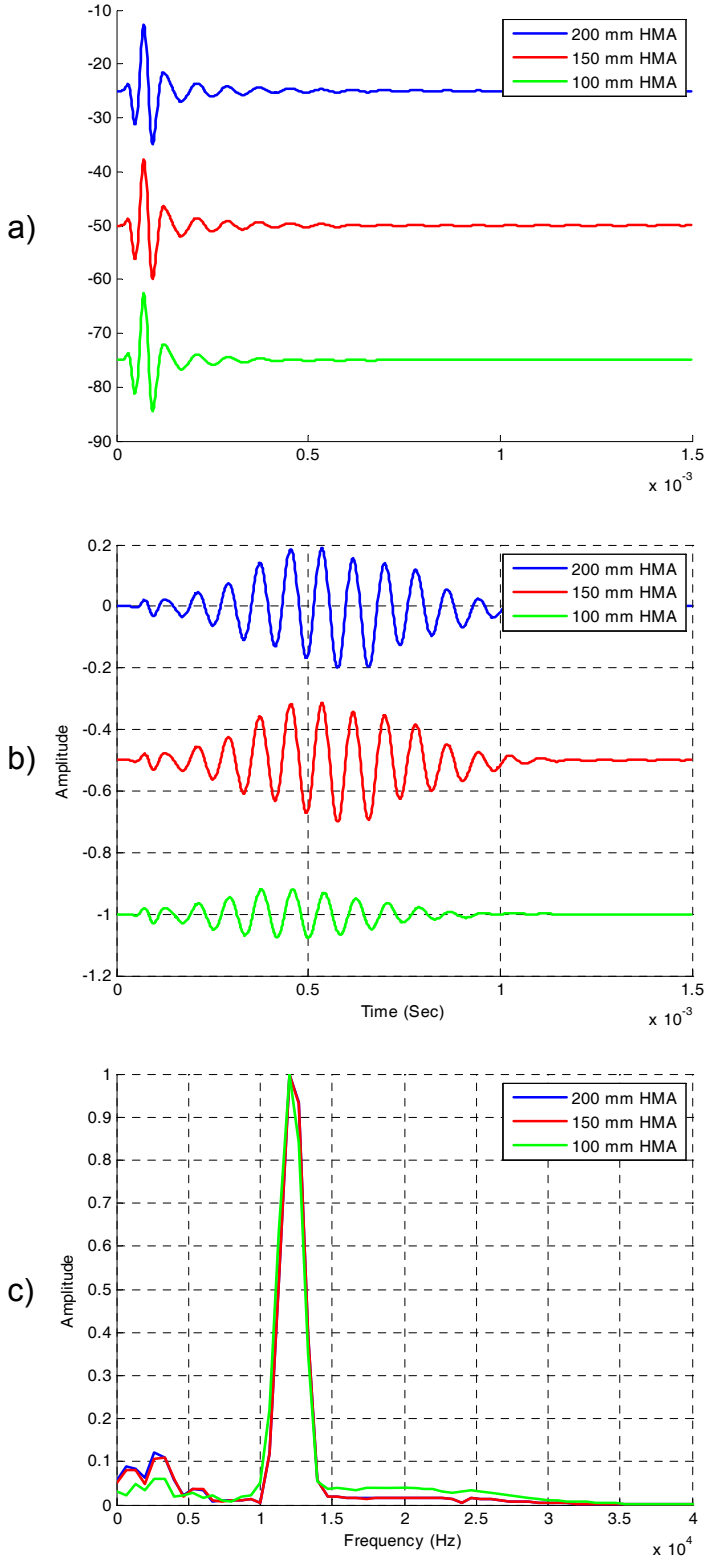


Figure 4.6: Impact of Thickness of HMA Layer, Comparison of: a) Time Record Signals, b) Time Record after Applying the Blackman-Harris Window, c) Frequency Spectra of Signals.

## 4.2 USW EVALUATION OF RESULTS

The impact of the interface condition on the dispersion curves from the USW method is shown in Figure 4.7a. For this case, a defect of 0.50 by 0.50 at a depth of 100mm and was used. The dispersion curves for the intact and partial-debonded cases are similar. However for the debonded section, a significant decrease in velocity at a depth of 0.1 m (defect of debonding) can be observed. The higher than normal phase velocities at shallow depths for the debonded area can be attributed to the interference of the reflected waves in the top 100 mm of the HMA. The average velocity was calculated for all cases and included in Figure 4.7b. For intact and partial debonding average values were very similar and slightly lower for total debonding. Thus, average velocities can readily be used as an indicator of the occurrence of debonding but not the partially debonded section.

The impact of the depth of defect on the dispersion curves are shown in Figure 4.8a. A total debonded defect of 0.50 by 0.50 was applied for this case. A defect at a depth of 50 mm to 100 mm can be readily detected. But when the defect is placed at a depth of 150 mm, it does not seem to be detectable with the USW method, as the dispersion curves from the intact and from a defect at a depth of 150 mm are quite similar. The same trend is observed for the case of average velocities (see Figure 4.8b).

The impact of the size of defect on dispersion curves is shown in Figure 4.9a. Defects were located at 100mm depth. For the 100 mm defect, the dispersion curve is similar to the dispersion curve from the intact section. Because of the size of the defect, both sensors (100 mm and 200 mm from the source) are placed on the intact HMA. The dispersion curve from the 300 mm defect shows a reduction in the phase velocity at a depth of 100 mm (depth of defect). At deeper depths, the phase velocity increases again. This can be explained because only the near sensor (100 mm from source) is placed on the defect and the farthest sensor is on intact HMA. For the 500 mm defect, where both sensors are placed on the defect, the dispersion curve demonstrates a significant decrease in the velocity below a depth of 100 mm. For the average velocities, results did not vary and only for the case of 500mm defect the average velocity decreases from the intact case (see Figure 4.9b).

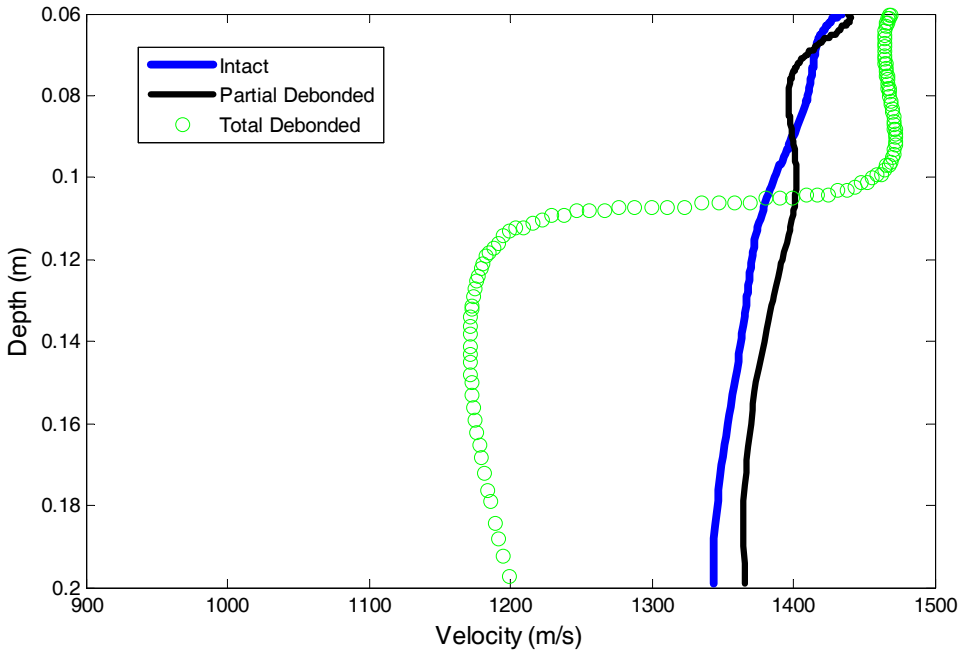


a)

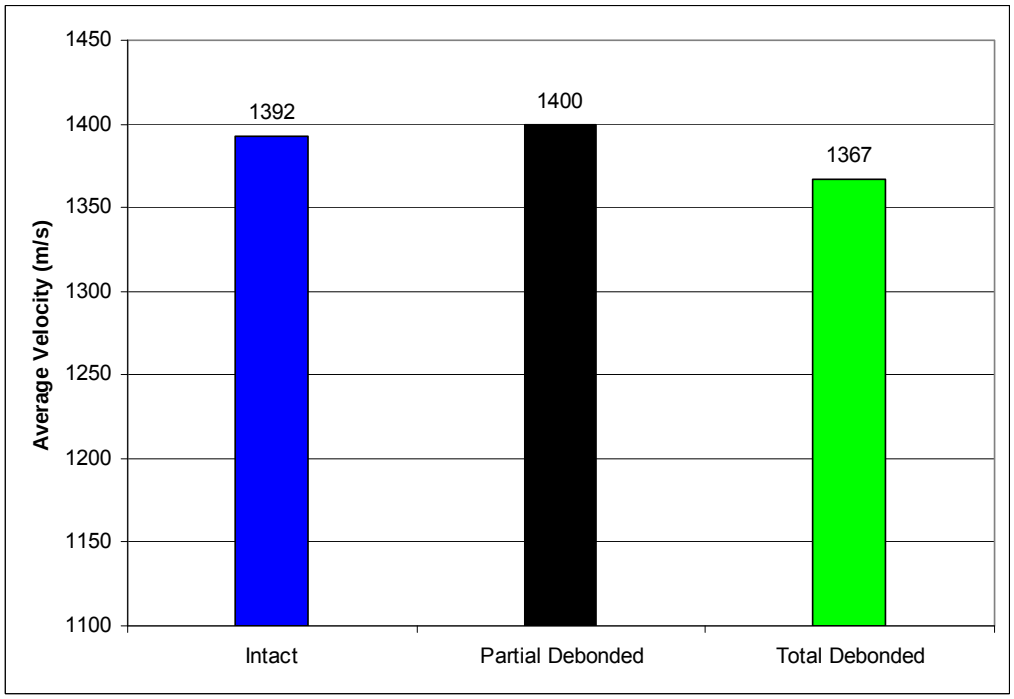


b)

Figure 4.7: Impact of Interface Condition, a) Dispersion Curves, b) Average Velocity of Surface Waves.

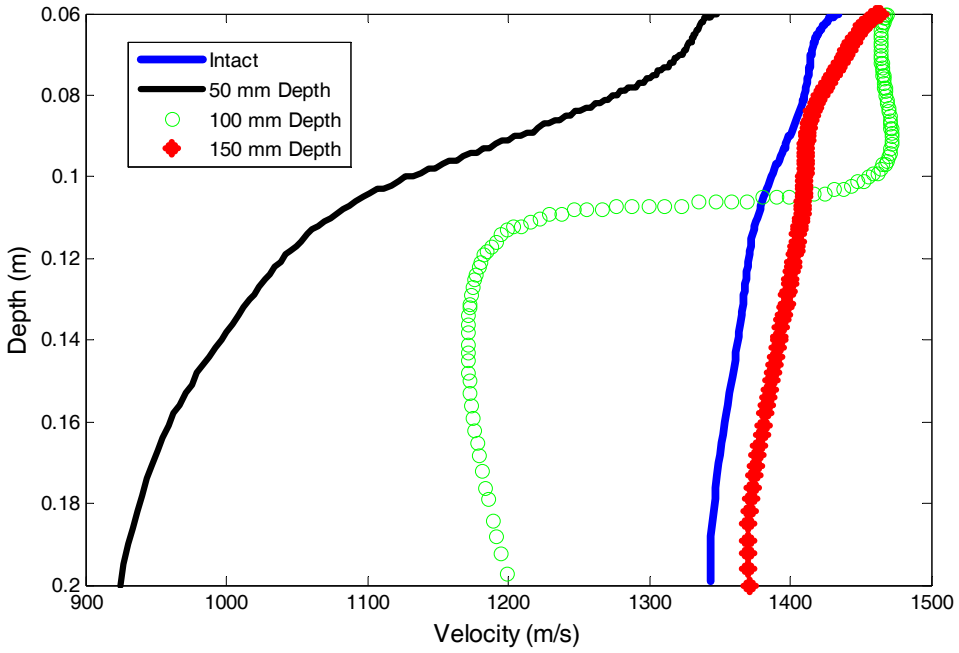


a)

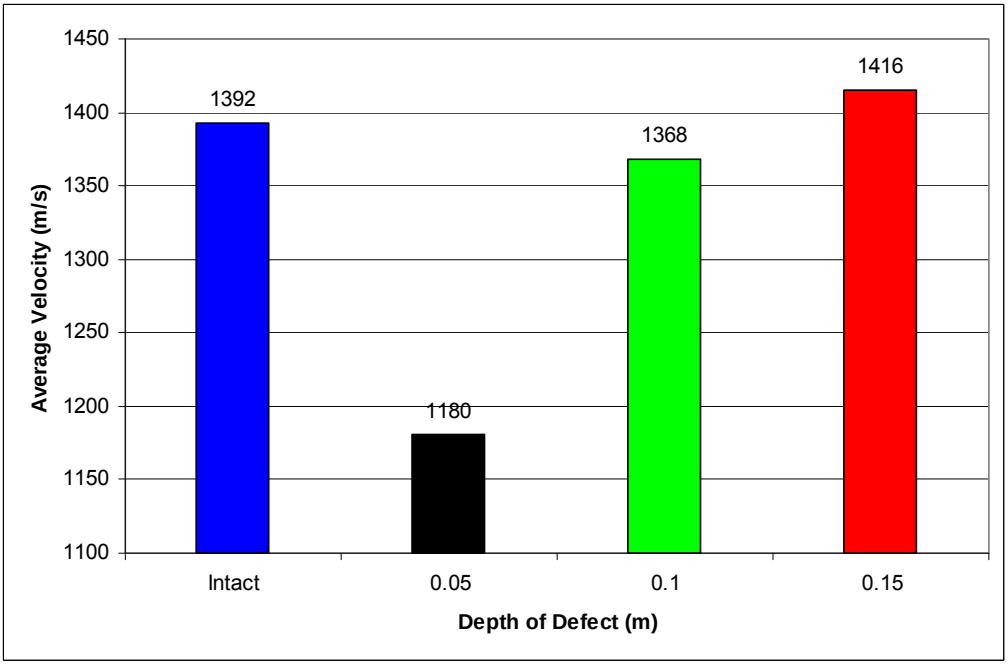


b)

Figure 4.8: Impact of Depth of Defect, a) Dispersion Curves, b) Average velocity of Surface Waves.

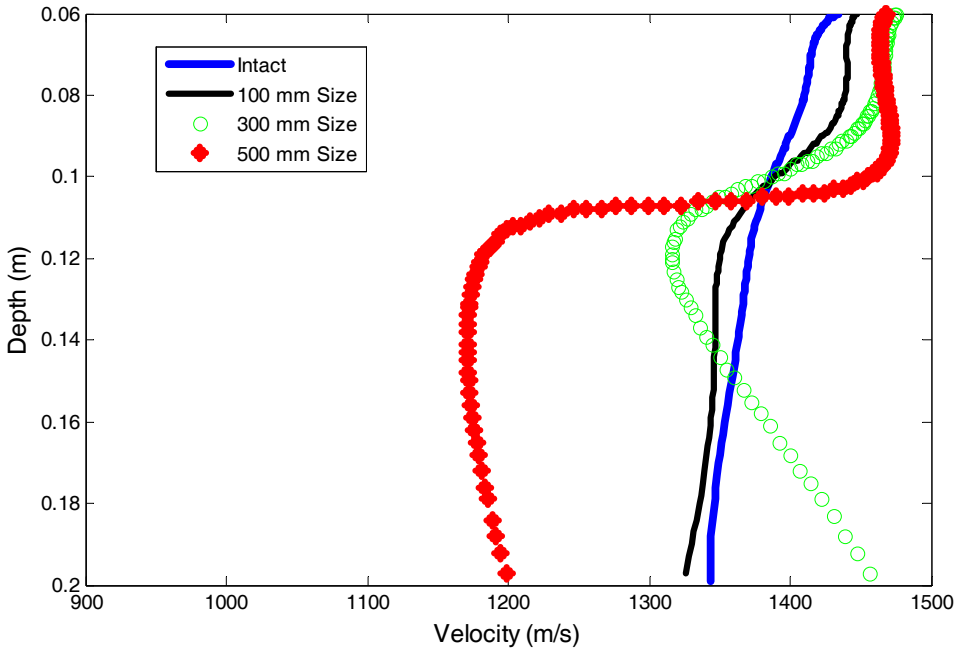


a)

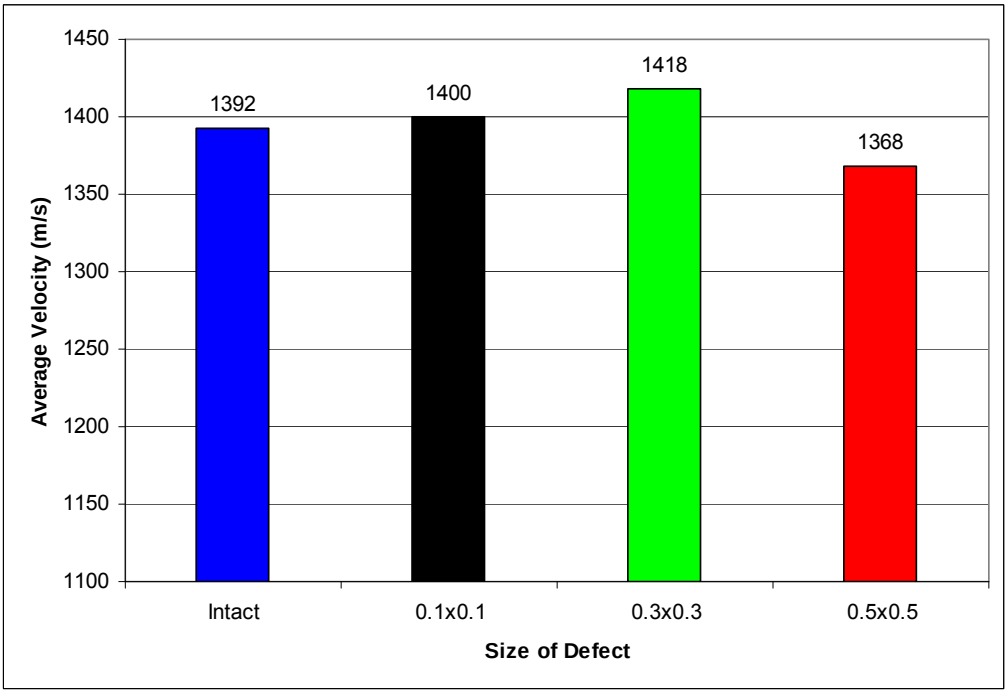


b)

Figure 4.9: Impact of Size of Defect, a) Dispersion Curves, b) Average Velocity of Surface Waves.

The modulus of the HMA does impact the results as anticipated, showing similar results to IE as illustrated in Figures 4.10a and 4.10b. However, the dispersion curves for all cases follow the same pattern starting with a constant velocity at shallow depths followed by a dramatic decrease in velocity at a depth corresponding to the location of the defect. Once again, this pattern shows the importance of adjusting the modulus of the layer with temperature. On this case, the average velocity linearly decreases with the drop in HMA modulus.

As for the IE method, the modulus of granular bases below the HMA does not seem to impact the results as shown in Figures 4.11a and 4.11b. Dispersion curves and average velocities for all cases are quite similar which indicates that change in modulus of elasticity of base does not have an impact on the USW results.

The impact of the thickness of the HMA layer in the range of 100 mm (depth of defect) to 200 mm is shown in Figure 4.12a. The dispersion curves for the 150 and 200 mm HMA thickness are similar, which indicates that the thickness of HMA below the defect does not impact the shape of the dispersion curves. For the 100 mm thick HMA, the dispersion curve is only slightly affected by the debonding. On the other hand average velocities are impacted by the different HMA thicknesses. The thicker the asphalt is the smaller the average velocity, as shown in Figure 4.12b.

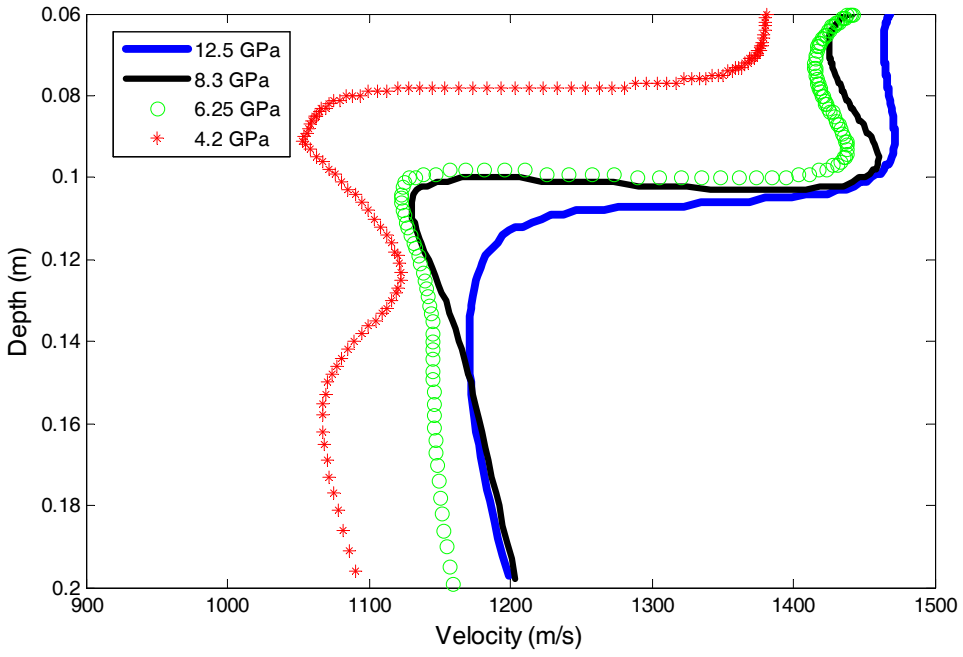


a)

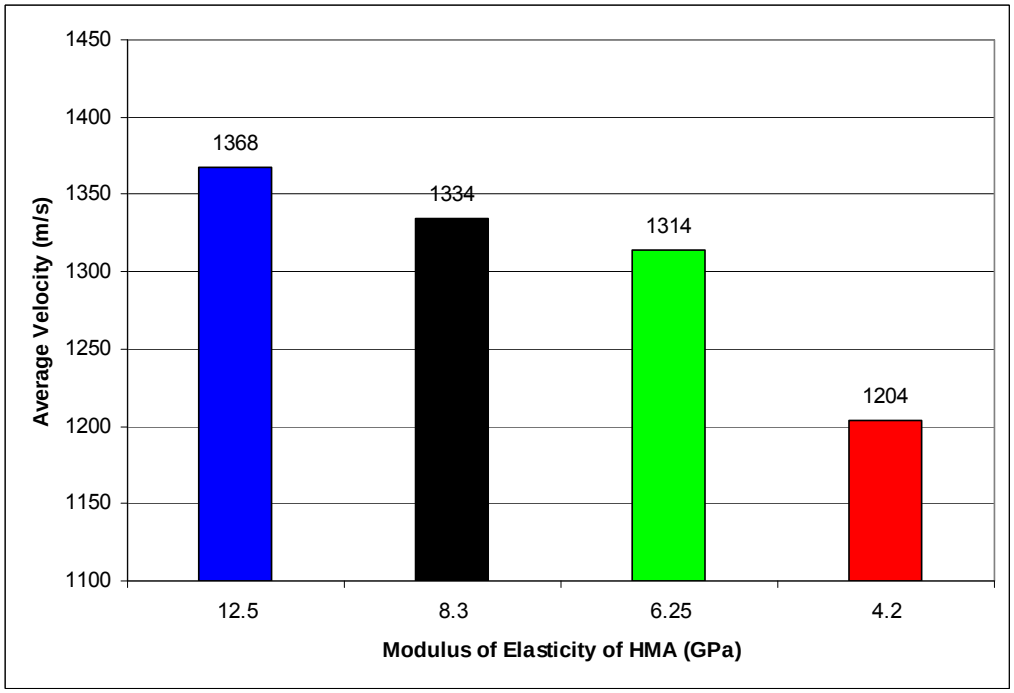


b)

Figure 4.10: Impact of Modulus of HMA, a) Dispersion Curves, b) Average Velocity of Surface Waves.

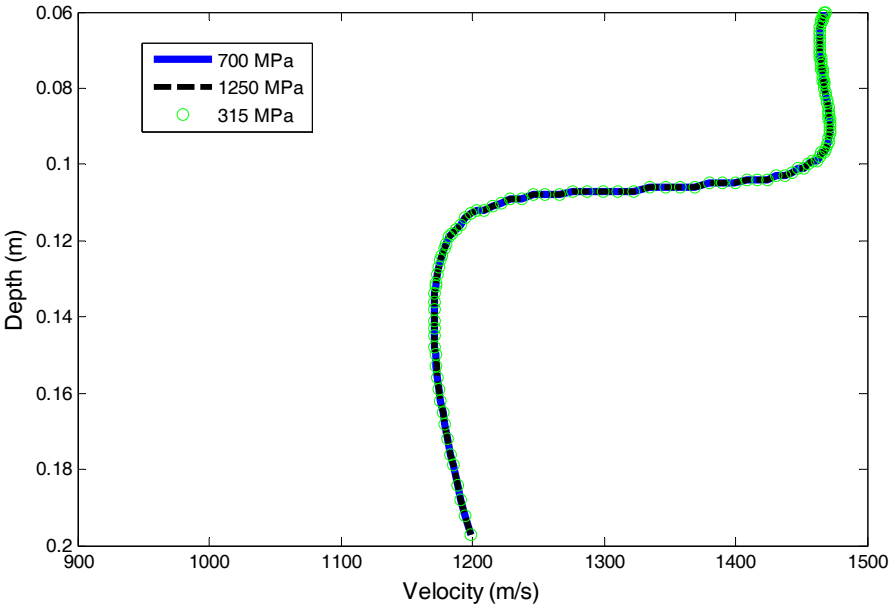


a)

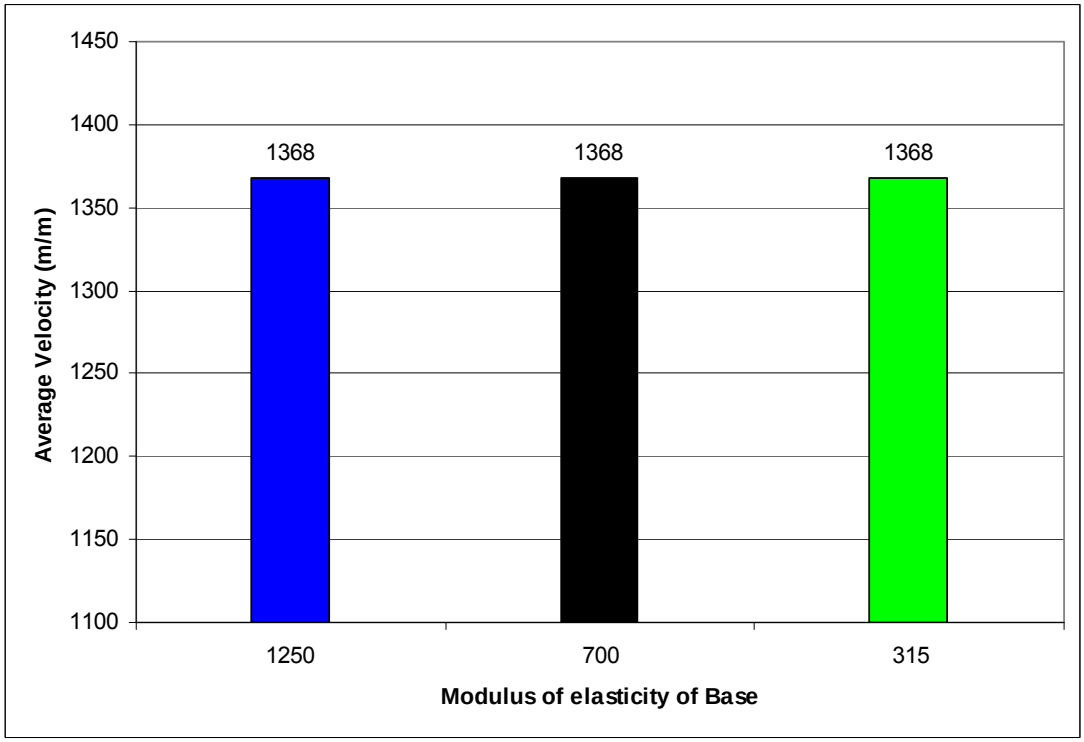


b)

Figure 4.11: Impact of Modulus of Elasticity of Base, a) Dispersion Curves, b) Average Velocity of Surface Waves.

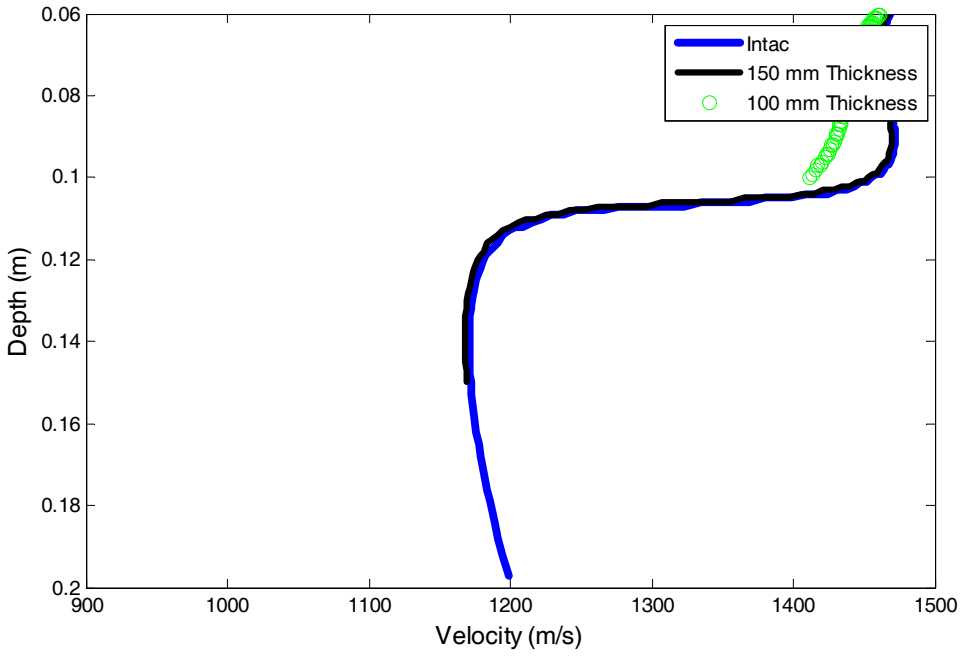


a)

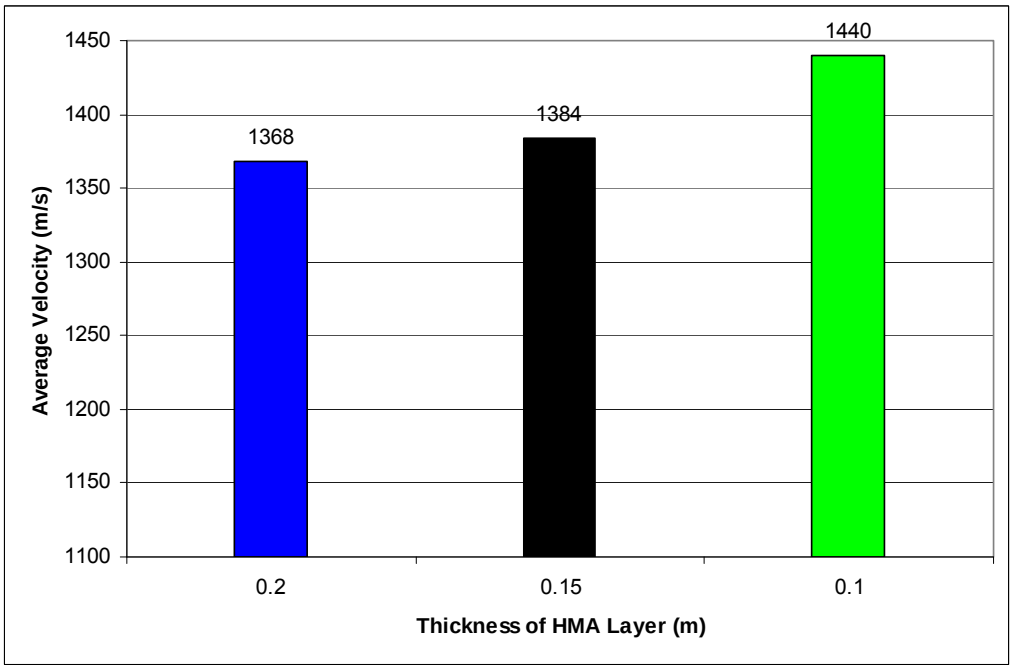


b)

Figure 4.12: Impact of Thickness of HMA Layer, a) Dispersion Curves, b) Average Velocity of Surface Waves.

## 4.3 IR EVALUATION OF RESULTS

The impact of the interface condition on the time records from the IR method is shown in Figure 4.13. The amplitude and shape of the time records change depending of the type of interface condition. The debonded case exhibits the largest amplitude followed by the partially debonded case. The ratio of the maximum amplitudes from the load and deflection are shown in Figure 4.13b. While a ratio of 0.4 obtained for the intact case, ratios of about 3 and 3.5 obtained for the partial debonded and total debonded cases respectively. As such, the IR method can readily detect the condition of the partially debonded and fully debonded cases.

The depth of the defect also significantly impacts the IR response as reflected in Figure 4.14a. The deeper the defect is, the lower the closer the amplitude ratio becomes to the intact case. Even though the defects at 50 and 100 mm depths are readily identified, the defect at a depth of 150 mm does not seem to be detectable relative to the intact case. This consequence is clearly reflected when FFT ratios were obtained (Figure 4.14b).

As reflected in Figure 4.15a, the defects less than 300 mm in size are not detectable with the IR method since their time records and their amplitude ratios are similar to the intact case. However, the 500 mm defect is readily detectable as illustrated on the higher ratio calculated (Figure 4.15b).

Similar to the other two methods, the change in the modulus of HMA has a pronounced effect on the peak amplitudes of the time records and the amplitude ratios (see Figures 4.16a and 4.16b). The geophone amplitude and FFT ratios increased as the HMA modulus decreased. This again indicates the importance of devising a site specific temperature correction relationship for this method.

Modulus of the base fortunately has a small effect on the results as shown in Figures 4.17a and 4.17b. The time records and amplitude ratios are quite similar which indicates that changes in the modulus of base do not have a significant impact on the interpretation of IR results.

The impact of the thickness of the HMA layer from 100 mm (depth of defect) to 200 mm is shown in Figure 4.18a. For 150 and 200 mm thickness the time records are comparable. However, for the case of 100 mm, the amplitude from the geophone signal was significantly smaller. The same trend was observed for the case of the amplitude ratios, as illustrated in Figure 4.18b.

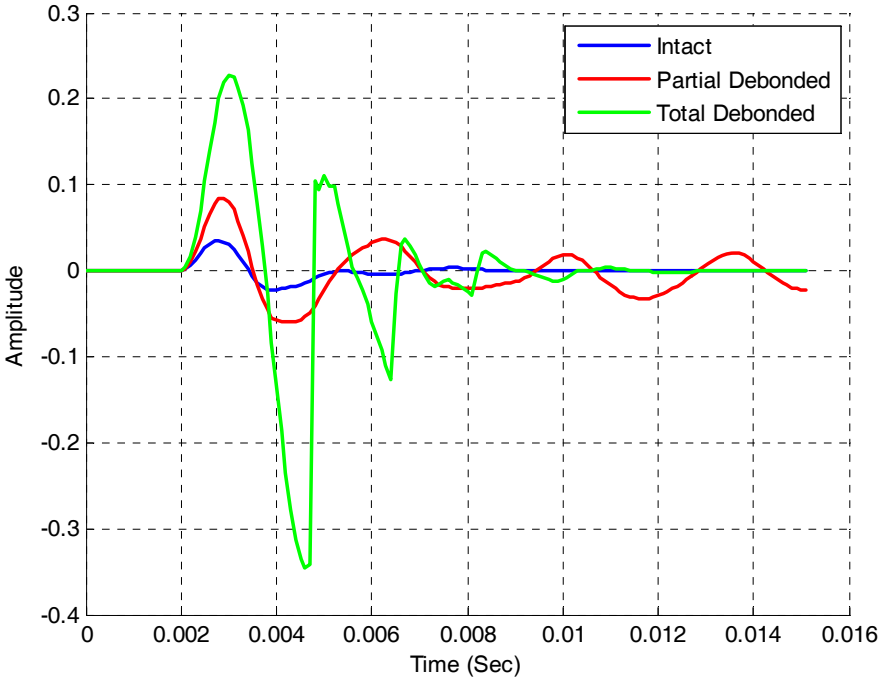


a)

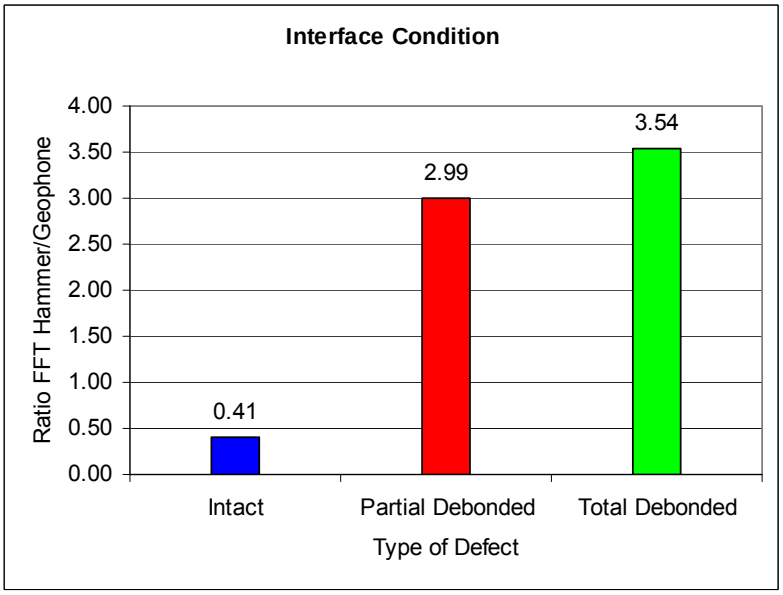


b)

Figure 4.13: Impact of Interface condition, a) Signal from Geophone, b) Comparison of Ratios FFT Hammer/Geophone.

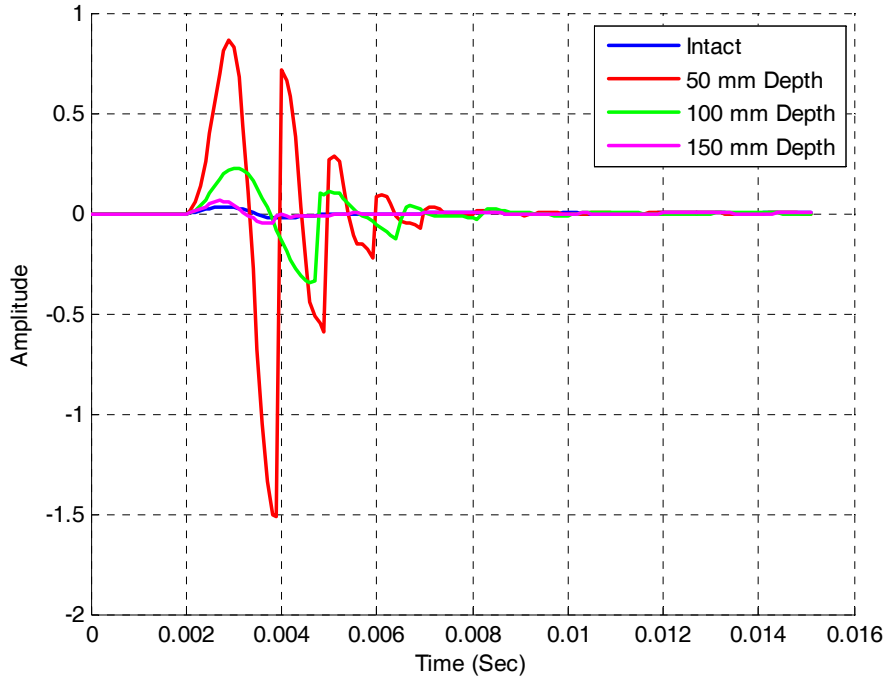


a)

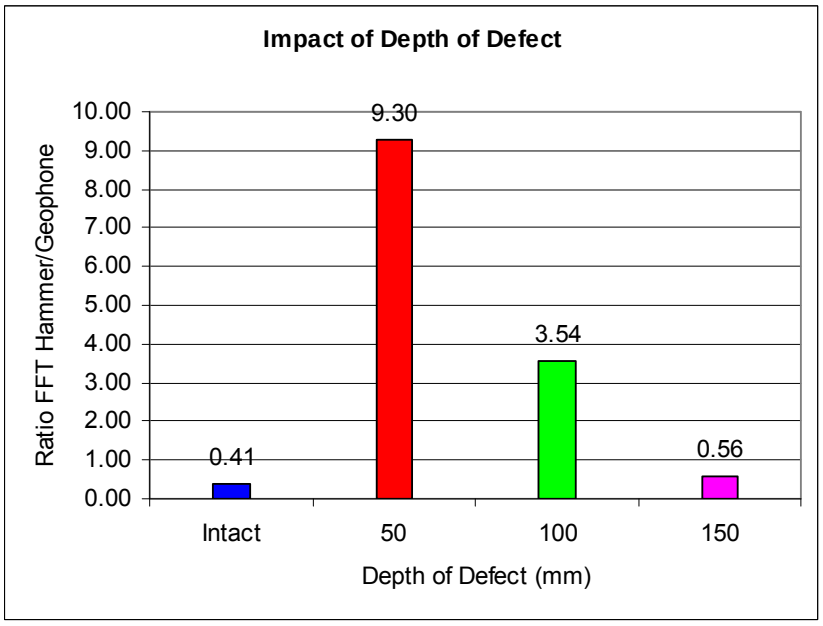


b)

Figure 4.14: Impact of Depth of Defect, a) Signal from Geophone, b) Comparison of Ratios FFT Hammer/Geophone.

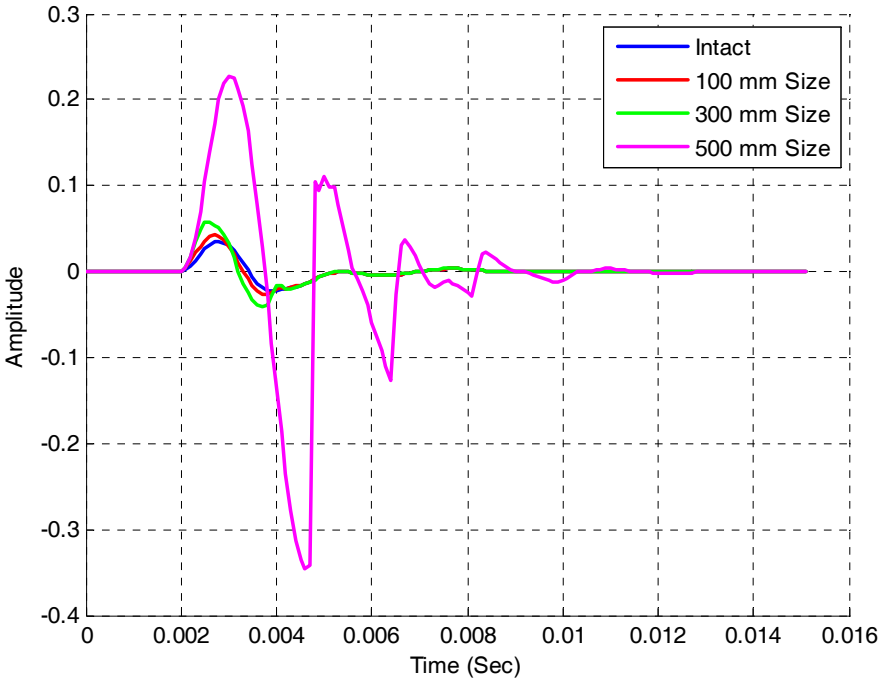


a)

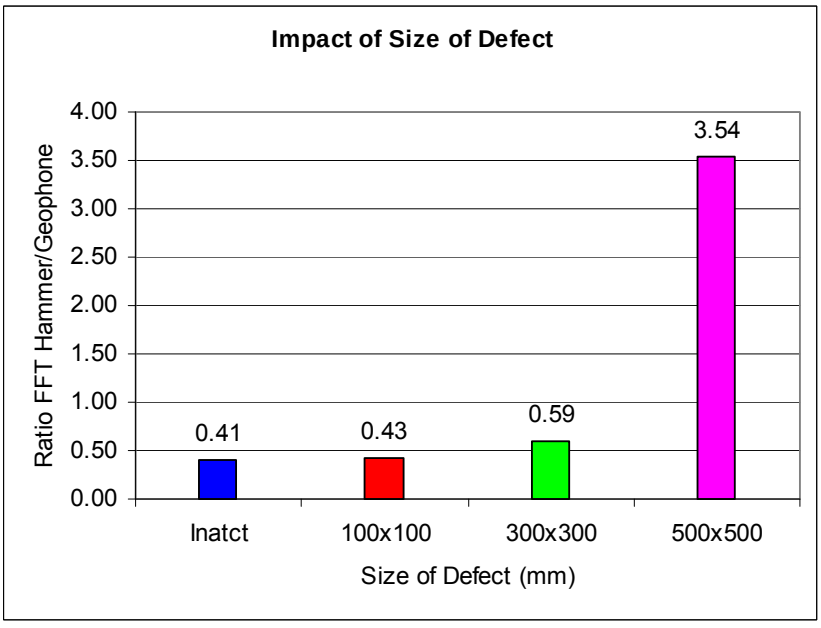


b)

Figure 4.15: Impact of Size of Defect, a) Signal from Geophone, b) Comparison of Ratios FFT Hammer/Geophone.

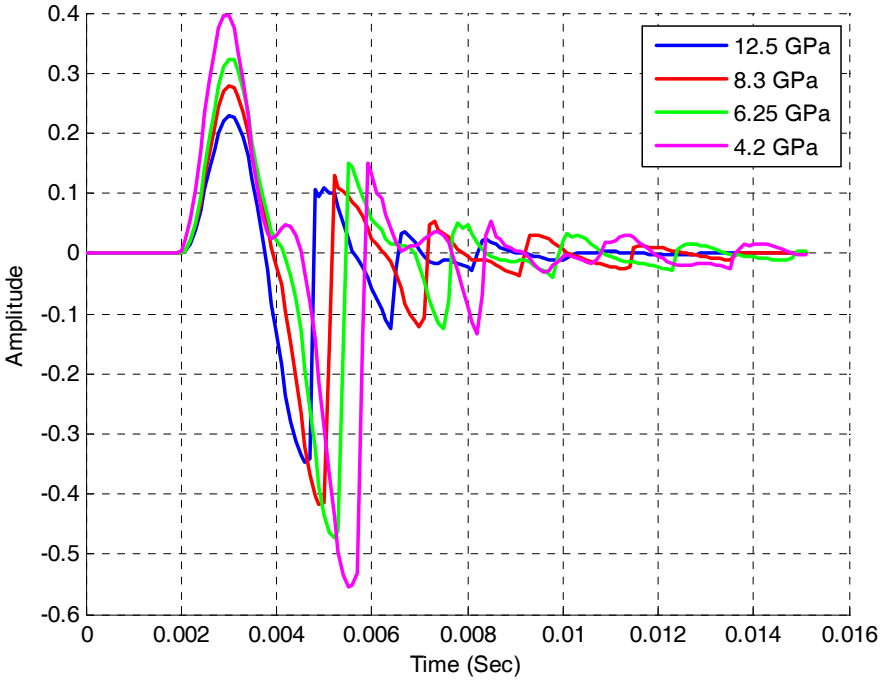


a)

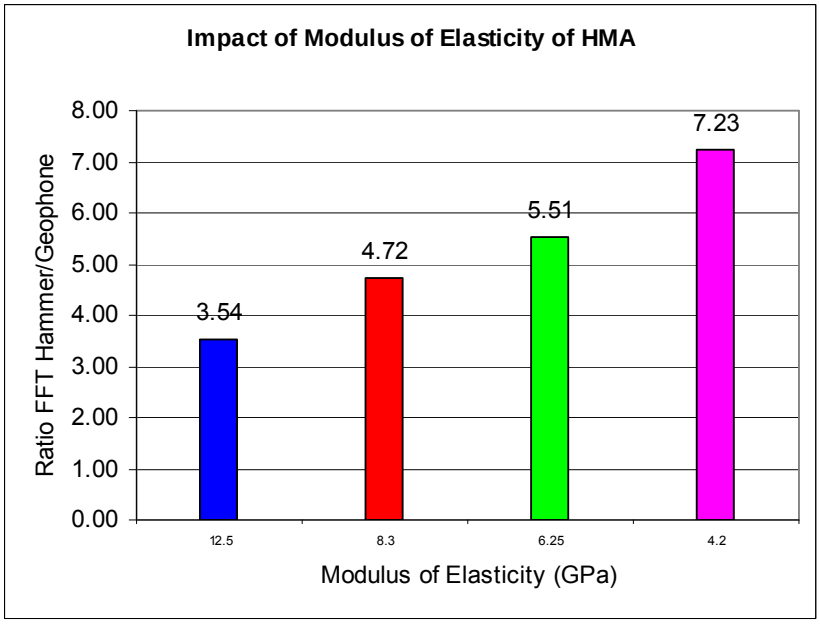


b)

Figure 4.16: Impact of Modulus of Elasticity of HMA, a) Signal from Geophone, b) Comparison of Ratios FFT Hammer/Geophone.

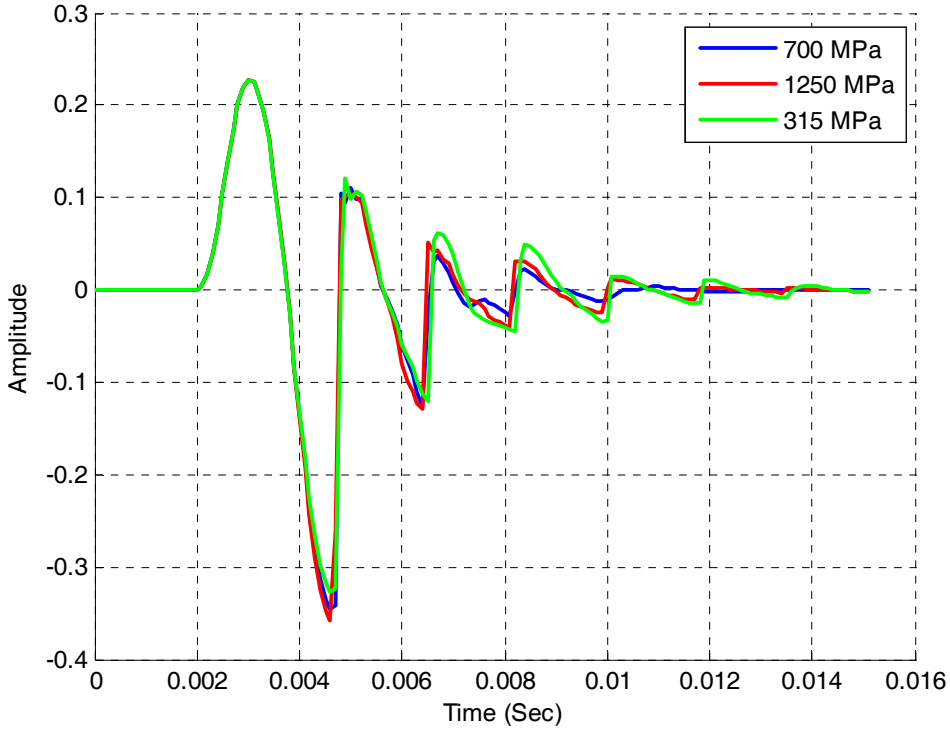


a)

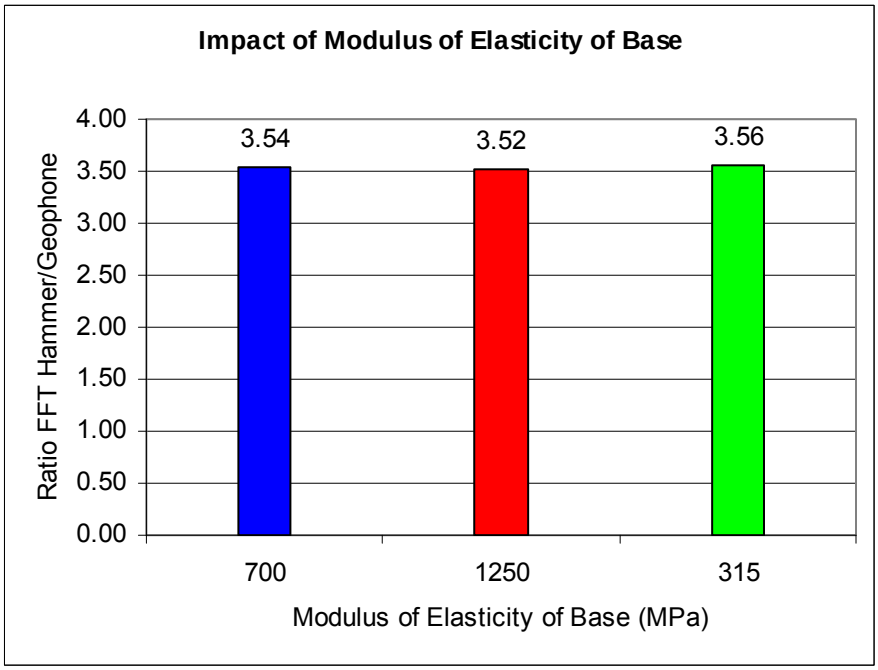


b)

Figure 4.17: Impact of Modulus of Elasticity of Base, a) Signal from Geophone, b) Comparison of Ratios FFT Hammer/Geophone.

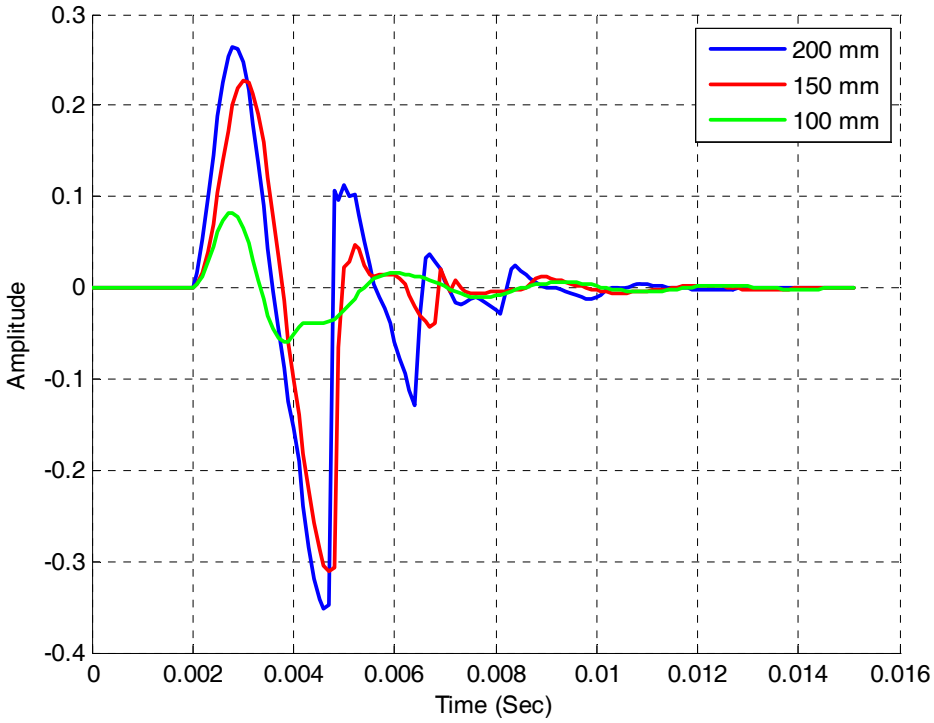


a)

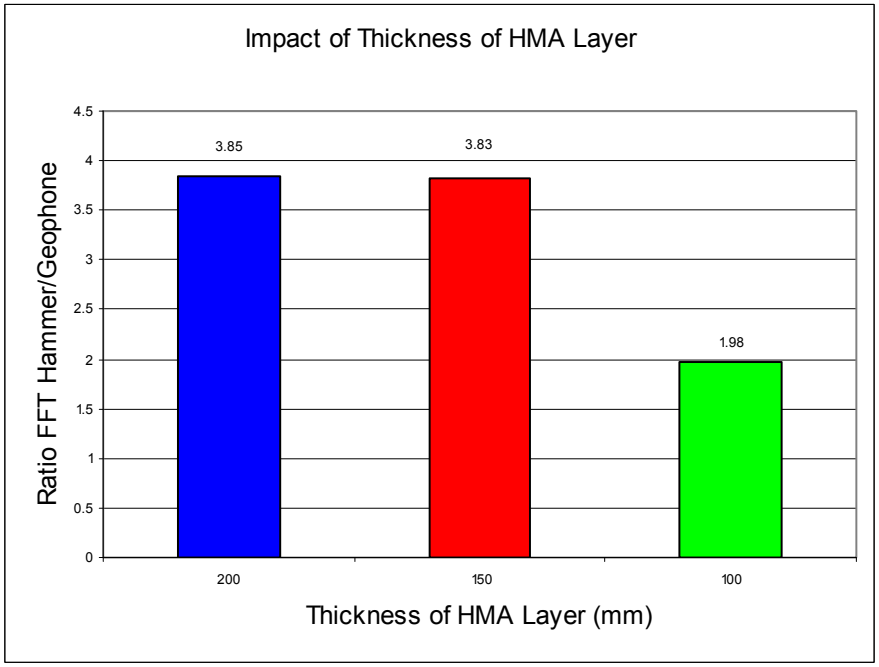


b)

Figure 4.18: Impact of Thickness of HMA, a) Signal from Geophone, b) Comparison of Ratios FFT Hammer/Geophone.

# Chapter 5: Conclusions and Recommendations

## CONCLUSIONS

Using LS-DYNA as a finite element method software, demonstrates to be an excellent tool to simulate the behavior of the results from the detection of delamination by using NDT methods.

Results of the IE-FEM were quite similar from those which were expected from theory. Although the FE results were not well related to those from the field, some similitude can be considered. It was found that all the variables have an impact on results obtained except for the change in modulus of elasticity of the base. There is a certain size of delamination in which the defect is more detectable. Moreover, shallow delaminations generated flexural mode.

Results of the USW-FEM indicated that FEM is a good tool to help on the detection of delamination of HMA layers by using USW. It was found that most of the variables have an impact on the results obtained from USW except for the change in modulus of elasticity of the base and the thickness of the HMA layer. In general it was found that delamination was manifested on this method as a drastic drop in velocity with a total recovery of the velocity. If the defect is close to the bottom edge of the HMA layer it can be difficult for USW to detect it. Also, it was observed that the place of the device greatly affected the signal obtained. If one sensor is placed above the defect and another sensor is away from it, unpredictable behavior of the signals was obtained.

Results of the IR-FEM can also be used as a complement for the detection of delamination by using IR method. From FE results it can be stated that IR is a simple method in which a large amplitude and a large FFT ratio indicate an enormous possibility to have a delamination under the point tested. If the delamination is large in dimensions and it is at a shallow depth, IR will detect that delamination. On the other hand, if the delamination is small and deep IR method most likely will have difficulties in detecting it. This is because the difference in amplitude and FFT ratio from an intact section and a delaminated section is not significant.

## RECOMMENDATIONS

Future work is needed for the FE model that was employed on this thesis. LS-DYNA is a complete software and even that the models gave excellent results some improvements to the FE model can be added, specifically in terms of the contact of the interfaces to generate the partial debonded condition. With a model improved it will be possible to obtain signals that are more comparable to the real world and thus creating a powerful tool in the detection of the delamination of HMA pavements by using IR, USW and IE methods. Also more variables can be added to the parametric study to understand the behavior of the signals from different case scenarios.

# References


Baker, M. R., Crain, K., Nazarian, S. (1995). "Determination of Pavement Thickness with a New Ultrasonic Device". Research Report 1966-1f, The Center for Geotechnical and Highway Materials Research, The University of Texas at El Paso, El Paso, Texas.

Bathe, K. J., Finite Element Procedures, 1996, Prentice-Hall, Inc., Englewood, NJ, 768-830.

Canestrari, F., Ferroti, G., Partl, M. N., Santagata, E. (2005). "Advanced Testing and Characterization of Interlayer Shear Resistance." Paper submitted for the TRB 84nd Annual Meeting,Washington DC.

Carino, N.J., 2001, "The Impact-Echo Method: an Overview." Proceedings of the 2001 Structures Congress & Exposition, May 21-23, 2001,Washington, D.C., American Society of Civil Engineers, Reston, Virginia (2001), 18 p.

Hammons, M. I., Von Quintus, H., Maser, K., and Nazarian, S. (2005). "Detection of stripping in hot mix asphalt." Applied Research Associates Project Number 16355, prepared for: Office of Materials and Research, Georgia Department of Transportation.

Kulkarni, M. B. (2004) "Effect of tack and prime coats, and bag-house fines on composite asphalt pavements." Ph.D. Dissertation, North Carolina State University, Raleigh, NC.

Kruntcheva, M. R., Collop, A. C., and Thom, N. H. (2005). "Effect of Bond Condition on Flexible Pavement Performance." Journal of Transportation Engineering, Volume 131, Issue 11, pp. 880-888, November 2005.

Kruntcheva, M. R., Collop, A. C. and Thom, N. H. (2004). "Feasibility of assessing bond condition of asphalt concrete layers with dynamic nondestructive testing." Journal of Transportation Engineering, Vol. 130, No. 4.

Medina, R. and Garrido, M (2007). Improving Impact-echo Method by Using Cross-spectral Density. Journal of Sound and Vibration, Volume 304, Issue 3-5, p. 769-778.

Mejia, D., Celaya, M., Iyer, S., Rao, C., Shokouhi, P., Nazarian, S.(2008). "A Work Plan toward Evaluation of Technologies to Assess Presence and Extent of Delamination of HMA Airfield Pavements." Research Project 06-04, conducted for: Airfield Asphalt Pavement Technology Program in cooperation with the Federal Aviation Administration, Center for Transportation Infrastructure Systems The University of Texas at El Paso El Paso, TX.

Nazarian, S., Baker, M. R., and Crain, K. (1993). ''Developing and Testing a Seismic Pavement Analyzer.'' Technical Report SHRP-H-375, Strategic Highway Research Program, Washington, D.C.

Nazarian, S.,Baker M., R., and Crain. K. (1997). "Assessing Quality of Concrete with Wave Propagation Techniques," Materials Journal, ACI, Farmington Hills, MI, Vol. 94 (4) 296- 306

Romanoschi, S. A., Metcalf, J. B. (2002). "The Characterization of Asphalt Concrete Layer Interfaces". Ninth International Conference of Asphalt Pavements, International Society for Asphalt Pavements.

Romanoschi, S. A., Metcalf, J. B. (2001). "The Effects of Interface Condition and Horizontal Wheel Loads on the Life of Flexible Pavement Structures". Transportation Research Record No. 1778. Transportation Research Board.

Sangiorgi, C., Collop, A., C. and Thom, N., H. (2003) "A nondestructive impulse hammer for evaluating the bond between asphalt layers in a road pavement." Non Destructive Testing in Civil Engineering, International Symposium, Liverpool, UK.

Sansalone, M. and Carino, N., J.. 1986. "Impact-Echo: A Method for Flaw Detection in Concrete Using Transient Stress Waves," Report NBSIR 86-3452, Gaithersburg, MD.

Sansalone, M. J., Streett, W.B., (1997). "Impact-Echo Nondestructive Evaluation of Concrete and Masonry" 1st Edition, Bullbrier Press, Ithaca, N.Y.

Shahin, M. Y., Kirchner, K., Blackmon, E.W., and Tomita, H., "Effect of Layer Slippage on Performance of Asphalt-Concrete Pavements," Transportation Research Record, no. 1095, pp. 79-85, 1986.

Shokouhi, P.,(2006) " Comprehensive Evaluation of Concrete Bridge Decks Using Impact Echo." Ph.D. Dissertation, Rutgers, The State University of New.

Yuan, D., Nazarian, S. (2000) "Feasibility of Detecting Flaws in Concrete Walls of Nuclear Power Plants" Research conducted for Jet Propulsion Laboratory The Center For Highway Materials Research, University of Texas at El Paso, El Paso, TX.

Zerwer, A.,Cascante, G., Hutchinson, J. (2002). "Parameter Estimation in Finite Element Simulation of Rayleigh Waves." Journal of Geotechnical & Environmental Engineering, ASCE, 128(3), 250-261.

# Vita

Dante Mejia Munoz was the third of four children. He was born at La Paz, Baja California Sur, México. He moved to Chihuahua Mexico, and he enrolled to The University of Chihuahua in the fall of 1999 and graduated with a bachelor degree in Civil Engineering in 2004. After graduating he worked in the construction field for three years. On 2007 he enrolled at the University of Texas at El Paso in the Master of Science program. While he was studying at UTEP he worked as a Research Assistant at the Center for Transportation Infrastructure Systems. He was inducted in to the National Civil Engineering Honor Society, Chi Epsilon. Now he is specializing in nondestructive methods and participated on a project from the Federal Aviation Administration.

Permanent address: Calle Cumbres de Majalca, n. 2032, Col. Cumbres II
Chihuahua, Chihuahua, 31217, MEXICO

This thesis/dissertation was typed by Dante Mejia Munoz.